processes

MDPI

Article

Maximum Power Point Tracking Constraint Conditions and Two Control Methods for Isolated Photovoltaic Systems

Jingxun Fan [1,2], Shaowu Li [1,*], Sanjun Liu [1,*], Xiaoqing Deng [1,3] and Xianping Zhu [1,4]

1 College of Intelligent Systems Science and Engineering, Hubei Minzu University, Enshi 445000, China; jingxun_fan@163.com (J.F.)
2 Jiangmen Pengjiang Power Supply Bureau of Guangdong Power Grid Co., Ltd., Jiangmen 529000, China
3 Hubei Chuangsinuo Electrical Technology Corp., Enshi 445000, China
4 Guilin Power Supply Bureau of Guangxi Power Grid Co., Ltd., Guilin 541000, China
* Correspondence: xidu_surfer@163.com (S.L.); liusanjinbox1@126.com (S.L.)

Abstract: A maximum power point (MPP) always exists in photovoltaic (PV) cells, but a mismatch between PV system circuit parameters, weather conditions and system structure leads to the possibility that the MPP may not be tracked successfully. In addition, the introduction of an isolation transformer into a basic PV system allows for moderate values of the converter duty cycle and electrical isolation. However, there is no comprehensive research on MPPT (maximum power point tracking) constraint conditions for different isolated PV systems, which seriously hinders the application of isolated PV systems and the development of a related linear control theory. Therefore, in this paper, the overall mathematical models of different isolated PV systems are first established based on the PV cell engineering model and the MPP linear model, and then, two sets of constraint conditions are found for the successful realization of MPPT. These MPPT constraint conditions (MCCs) describe in detail the direct mathematical relationships between PV cell parameters, weather conditions and circuit parameters. Finally, based on the MPP linear model and MCCs, two new MPPT methods are designed for isolated PV systems. Considering the MCCs proposed in this paper, a suitable range of load and transformer ratios can be estimated from the measured data of irradiance and temperature in a certain area, and the range of MPPs existing in PV systems with different structures can be estimated, which is a good guide for circuit design, theoretical derivation and product selection for PV systems. Meanwhile, comparative experiments confirm the rapidity and accuracy of the two proposed MPPT methods, with the MPPT time improving from 0.23 s to 0.03 s, and they have the advantages of a simple program, small computational volume and low hardware cost.

Keywords: isolated PV system; MPPT constraint conditions; linear cell model

check for updates

Citation: Fan, J.; Li, S.; Liu, S.; Deng, X.; Zhu, X. Maximum Power Point Tracking Constraint Conditions and Two Control Methods for Isolated Photovoltaic Systems. *Processes* **2023**, *11*, 3245. https://doi.org/10.3390/pr11113245

Academic Editors: Chenyu Wu, Zhongkai Yi and Chenhui Lin

Received: 30 September 2023
Revised: 27 October 2023
Accepted: 8 November 2023
Published: 17 November 2023

Copyright: © 2023 by the authors. Licensee MDPI, Basel, Switzerland. This article is an open access article distributed under the terms and conditions of the Creative Commons Attribution (CC BY) license (https://creativecommons.org/licenses/by/4.0/).

1. Introduction

To carry out a theoretical analysis and practical verification of a PV system, an accurate model of the PV cell should be established first. Nowadays, a large number of studies on PV systems and PV cells are carried out, and they have led to a lot of breakthroughs and innovations in mathematical and circuit model optimization, as well as MPPT and parameter extraction methods for PV cells. However, the model used cannot be completely compatible with the required accuracy, the complexity of the calculations and the environmental conditions [1]. There are nine commonly used circuit models and mathematical models of PV cells categorized in Ref. [2], which can accurately reflect the output characteristics of PV cells but are not convenient for engineering applications, so simplified engineering models of PV cells have been widely investigated [3]. Many scholars have investigated how to model PV cells using four important parameters (I_{sc}, V_{oc}, I_m and V_m) provided by manufacturers and, based on the derivation of the circuit model, to simplify the modeling process, which is called engineering modeling. Under standard test conditions (STC; solar irradiance S is 1000 W/m^2, and PV cell temperature T is 25 °C), the PV cell engineering model is obtained using Equations (1)–(3), where I, V, I_{sc}, V_{oc}, I_{m} and V_{m} represent the output current, voltage of the PV cell, short-circuit current, open-circuit voltage, MPP current and voltage of the PV cell at STC, respectively [4].

$$I = I_{\mathrm{sc}}\left[1 - C_1\left(\mathrm{e}^{\frac{V}{C_2 V_{\mathrm{oc}}}} - 1\right)\right] \tag{1}$$

$$C_1 = \left(1 - \frac{I_{\mathrm{m}}}{I_{\mathrm{sc}}}\right)\mathrm{e}^{-\frac{V_{\mathrm{m}}}{C_2 V_{\mathrm{oc}}}} \tag{2}$$

$$C_2 = \frac{\frac{V_{\mathrm{m}}}{V_{\mathrm{oc}}} - 1}{\ln\left(1 - \frac{I_{\mathrm{m}}}{I_{\mathrm{sc}}}\right)} \tag{3}$$

However, when there are obstacles such as tall buildings and trees, the illumination of PV modules is no longer uniform, resulting in partial shadow problems in which the power curve has multiple peaks. So, it is necessary to establish a PV model under partial shadow conditions and to simulate and analyze its output characteristics [5,6]. This is a steady-state model of PV cells, but MPPT is a dynamic optimization process, so the dynamic characteristics of PV cells have also been studied in a number of ways [7]. All of the above models are nonlinear models of PV cells, which require complex iterations and calculations to extract parameters and conduct studies, so scholars have proposed some linearized models, such as segmented linear models, which replace the nonlinear PV relationship with multi-segmented linear equations through segmented linearization [8]. In [9], the authors proposed a new segmented linear shunt branch model that approximates the nonlinear *I-V* curve of a PV cell via an equivalent circuit. The segmented linearized model simplifies the workload in the nonlinear PV cell model and obtains comparable accuracy under certain conditions, but the number of segments must be increased in the segmented linear model if higher accuracy is required, which undoubtedly increases the computational complexity. The authors of [10] derived a linearized model that relates changes in the inputs to the system, such as irradiance and temperature, to its outputs, such as the array current and power. The authors of [11] derived a set of nonlinear state-space equations based on the average switching technique, which was implemented using MATLAB2016b. The authors of [12] linearized the voltage–current characteristics of PV cells at the MPP in order to completely remove the obstacle of nonlinear PV cells to the overall linearization of the PV system by proposing two equivalent linear models, the Thevenin equivalent model and the Norton equivalent model, as shown in Figure 1. In contrast, the MPP linear model can better overcome these problems in the segmented linear model. On this basis, it is feasible and reasonable to linearize the PV system as a whole, and the PV system can be conveniently studied using the traditional linear theory or law.

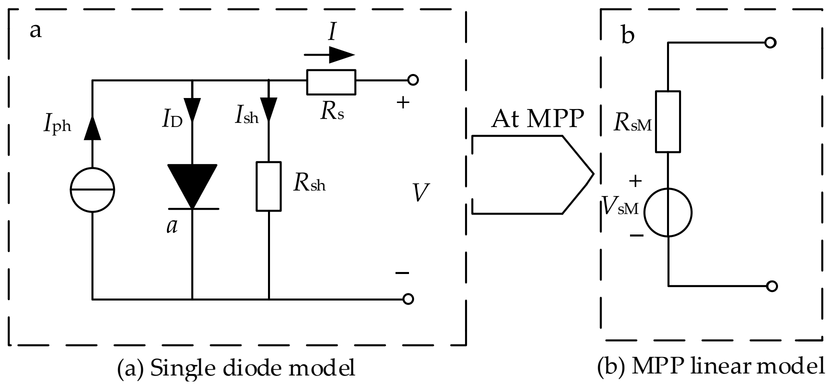

Figure 1. Relationship between single-diode model and MPP linear model.

The DC/DC converters in PV systems are categorized into non-isolated and isolated DC/DC converters. Non-isolated DC/DC converters, such as buck, boost, buck-boost and Sepic converters, are widely used as the MPPT control circuits of PV systems. Isolated DC/DC converters usually include forward, flyback, push–pull, half-bridge and full-bridge converters. The introduction of an isolation transformer into a basic non-isolated DC/DC converter can realize electrical isolation between the converter's input power supply and load. Meanwhile, it can improve the safety and reliability of converter operation and electromagnetic compatibility. In addition, it can make the duty cycle of the DC/DC converter change near a moderate value. Usually, in this case, a high boosted voltage can be achieved by using a high-transformation-ratio transformer and a voltage multiplier [13]. The analysis shown in Reference [14] verifies that isolation not only ensures safety but also increases the MPPT capability. Meanwhile, it shows that isolated converters have the highest MPPT capability without considering the hardware implementation.

At present, MPPT methods can be classified into five categories: (1) classical methods, such as perturbation observation, constant voltage and conductance increment methods [15]; (2) intelligent methods, such as artificial neural networks (ANNs), fuzzy logic controllers (FLCs) and sliding-mode control (SMC) [16,17]; (3) optimization methods, such as cuckoo search (CS), the particle swarm algorithm (PSO), the gray wolf algorithm (GWO), the ant colony algorithm (ACO) and the artificial bee colony algorithm (ABC) [18,19]; (4) hybrid methods, such as fuzzy particle swarm optimization (FPSO) and the adaptive neuro-fuzzy inference system (ANFIS) [20]; (5) other methods, such as the variable-weather parameter (VWP) method [21]. Under specific environmental conditions and requirements, good performance can be obtained with all five of the above-mentioned MPPT methods. However, the nonlinear model of the PV cell is one of the fundamental reasons why the linear control theory cannot be widely applied in the MPPT control of PV systems at present. And since the MPP must always exist in the process of use, it is easy to cause errors if its constraints are not analyzed. In order to solve this problem, some expressions have been proposed in Reference [22] to ensure the existence of the MPP in PV systems with buck, boost, buck/boost and other non-isolated DC/DC converters.

Therefore, the research objective of this paper is as follows: to find the relationship between the circuit parameters and the control signals of an isolated PV system by directly utilizing the weather conditions so as to find the range of circuit parameters for which it is capable of successful MPPT control and, accordingly, to propose two new MPPT methods.

The innovations and contributions of this work are as follows:

(1) The mathematical models of isolated PV systems are established, and the mathematical relationships between the output power of the PV systems and the weather conditions are found.
(2) The MCCs of isolated PV systems are found based on the engineering model and the MPP linear model. The relationships between MCCs and the weather conditions, circuit parameters and system structure are obtained.
(3) The practicality of the MPPT control algorithm can be enhanced. The problem of MPPT failure can be avoided by fully considering the MCCs in the design and improvement of the MPPT algorithm. Therefore, two MPPT methods, which are applicable to different PV system structures, are proposed to improve the stability, applicability and rapidity of MPPT control.

The section arrangement of this paper is as follows: Two MPPT constraint conditions and two new MPPT methods are presented in Section 2. Some simulation experiments are presented in Section 3. Finally, a discussion and some conclusions are given in Sections 4 and 5, respectively.

2. Materials and Methods

2.1. Integrative Model of Isolated PV Systems

The structure of the isolated PV system is shown in Figure 2. I and V denote the output current and voltage of the PV cell, respectively. I_o and V_o denote the output current and output voltage of the isolated DC/DC converter, respectively. R_i and R_L denote the equivalent resistances after the PV cell and after the isolated DC/DC converter, respectively.

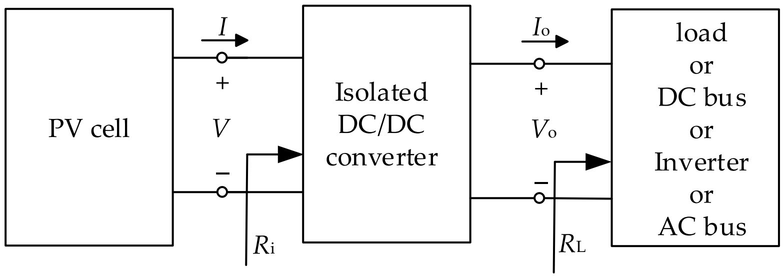

Figure 2. Isolated PV system structure.

The basic circuits of isolated DC/DC converters include the forward converter, flyback converter, half-bridge converter, full-bridge converter and push–pull converter. They are associated with the PV cell to produce the PV-Forward system, PV-Flyback system, PV-Half-bridge system, PV-Full-bridge system and PV-push–pull system, respectively. The isolated DC/DC converter is generally connected to a resistor, DC bus, inverter or AC bus (shown in Figure 3). The different system structures also lead to differences in the mathematical model and MPPT method.

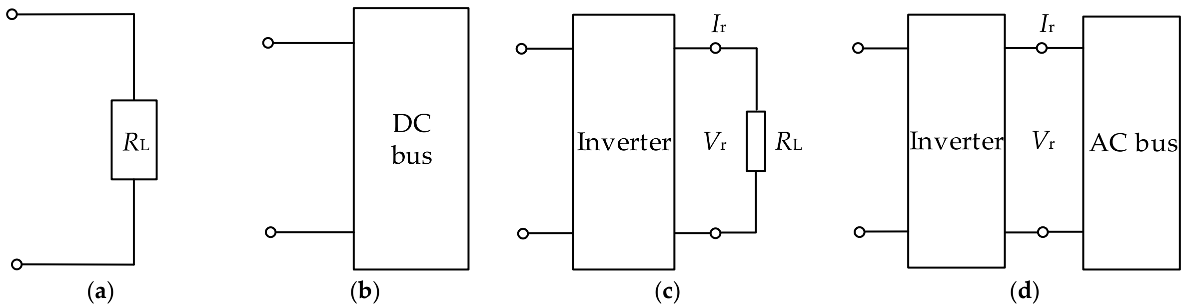

Figure 3. Four types of output. (**a**) Load; (**b**) DC bus; (**c**) inverter; (**d**) AC bus.

In order to derive a theoretical mathematical model, two assumptions need to be made for isolated PV systems:

(1) All circuit components are ideal;
(2) The isolated DC/DC converter operates in the continuous-current mode (CCM).

Firstly, according to Figure 2, it can be obtained by the power balance relationship:

$$VI = V_o I_o = P_o \tag{4}$$

$$R_i = \frac{V}{I} \tag{5}$$

$$R_L = \frac{V_o}{I_o} \tag{6}$$

P_o denotes the output power of the PV system.

The input-and-output-voltage relationships of forward, flyback, half-bridge, full-bridge and push–pull converters can be expressed by Equations (7)–(11), respectively [23]. D denotes the duty cycle of the PWM wave for the isolated DC/DC converter, and the isolation transformer ratio n is equal to N_1/N_2.

$$V_o = \frac{DV}{n} \tag{7}$$

$$V_o = \frac{DV}{n(1-D)} \tag{8}$$

$$V_o = \frac{DV}{n} \tag{9}$$

$$V_o = \frac{2DV}{n} \tag{10}$$

$$V_o = \frac{DV}{n} \tag{11}$$

It can be seen that Equations (7), (9) and (11) are the same, which means that the input–output-voltage relationships are the same for forward, half-bridge and push–pull converters.

According to Figure 2, Equation (12) is satisfied.

$$P_o = \frac{V_o^2}{R_L} \tag{12}$$

The mathematical model of the PV-Forward system can be obtained by combining Equations (1), (4), (7) and (12).

$$P_o = \frac{n^2 R_L I_{sc}^2}{D^2}\left[1 - C_1\left(e^{\frac{n\sqrt{P_o R_L}}{C_2 D V_{oc}}} - 1\right)\right]^2 \tag{13}$$

Since the forward, half-bridge and push–pull converters have the same input–output-voltage relationships, the mathematical models of the PV-Forward, PV-Half-bridge and PV-Push–pull systems are also the same, all of which are expressed in Equation (13) and will not be repeated below.

Similarly, the mathematical models of the PV-Flyback and PV-Full-bridge systems can also be obtained.

$$P_o = \frac{n^2 R_L I_{sc}^2 (1-D)^2}{D^2}\left[1 - C_1\left(e^{\frac{n(1-D)\sqrt{P_o R_L}}{C_2 D V_{oc}}} - 1\right)\right]^2 \tag{14}$$

$$P_o = \frac{n^2 R_L I_{sc}^2}{2D^2}\left[1 - C_1\left(e^{\frac{n\sqrt{P_o R_L}}{2C_2 D V_{oc}}} - 1\right)\right]^2 \tag{15}$$

For the DC bus, Equation (16) is satisfied.

$$V_o = V_{Dbus} \tag{16}$$

The mathematical model of the PV-Forward-Dbus system can be obtained by combining Equations (1), (4), (7) and (16).

$$P_o = \frac{n V_{Dbus} I_{sc}}{D}\left[1 - C_1\left(e^{\frac{n V_{Dbus}}{C_2 D V_{oc}}} - 1\right)\right] \tag{17}$$

Similarly, the mathematical models of the PV-Flyback-Dbus and PV-Full-bridge-Dbus systems can also be obtained.

$$P_o = \frac{n V_{Dbus} I_{sc} (1-D)}{D}\left[1 - C_1\left(e^{\frac{n V_{Dbus}(1-D)}{C_2 D V_{oc}}} - 1\right)\right] \tag{18}$$

$$P_o = \frac{n V_{Dbus} I_{sc}}{2D}\left[1 - C_1\left(e^{\frac{n V_{Dbus}}{2C_2 D V_{oc}}} - 1\right)\right] \tag{19}$$

The mathematical models of the inverter (SPWM control) and AC load can be represented by Equations (20) and (21), respectively. M denotes the SPWM wave modulation ratio. V_r and I_r denote the RMS values of the output AC voltage and AC current for the inverter, respectively.

$$V_r = \frac{MV_o}{\sqrt{2}} \tag{20}$$

$$R_L = \frac{V_r}{I_r} \tag{21}$$

The mathematical model of the PV-Forward-INV system can be obtained by combining Equations (1), (4), (7), (20) and (21).

$$P_o = \frac{2n^2 R_L I_{sc}^2}{D^2 M^2}\left[1 - C_1\left(e^{\frac{n\sqrt{2P_o R_L}}{C_2 DMV_{oc}}} - 1\right)\right]^2 \tag{22}$$

Similarly, the mathematical models of the PV-Flyback-INV and PV-Full-bridge-INV systems can also be obtained.

$$P_o = \frac{2n^2 R_L I_{sc}^2 (1-D)^2}{D^2 M^2}\left[1 - C_1\left(e^{\frac{n(1-D)\sqrt{2P_o R_L}}{C_2 DMV_{oc}}} - 1\right)\right]^2 \tag{23}$$

$$P_o = \frac{n^2 R_L I_{sc}^2}{2D^2 M^2}\left[1 - C_1\left(e^{\frac{n\sqrt{2P_o R_L}}{2C_2 DMV_{oc}}} - 1\right)\right]^2 \tag{24}$$

For the AC bus, Equation (25) is satisfied.

$$V_r = V_{Abus} \tag{25}$$

The mathematical model of the PV-Forward-INV-Abus system can be obtained by combining Equations (1), (10), (13) and (25).

$$P_o = \frac{\sqrt{2}nV_{Abus}I_{sc}}{DM}\left[1 - C_1\left(e^{\frac{\sqrt{2}nV_{Abus}}{C_2 DMV_{oc}}} - 1\right)\right] \tag{26}$$

Similarly, the mathematical models of the PV-Flyback-INV-Abus and PV-Full-bridge-INV-Abus systems can also be obtained.

$$P_o = \frac{\sqrt{2}nV_{Abus}I_{sc}(1-D)}{DM}\left[1 - C_1\left(e^{\frac{\sqrt{2}nV_{Abus}(1-D)}{C_2 DMV_{oc}}} - 1\right)\right] \tag{27}$$

$$P_o = \frac{\sqrt{2}nV_{Abus}I_{sc}}{2DM}\left[1 - C_1\left(e^{\frac{\sqrt{2}nV_{Abus}}{2C_2 DMV_{oc}}} - 1\right)\right] \tag{28}$$

Equations (13)–(15), (17)–(19), (22)–(24) and (26)–(28) are the theoretical basis for the MCCs of PV systems with these five isolated DC/DC converters connected to the load, DC bus, inverter and AC bus, respectively.

It can be concluded that P_{omax} appears in the slope of the curve at 0. Therefore, in order to find the MCCs of PV systems with different structures, their mathematical models are analyzed by substituting each of them into Equation (29).

$$\frac{dP_o}{dD} = 0 \tag{29}$$

For the PV-Forward, PV-Flyback, PV-Full-bridge and PV-Forward-Dbus systems, substituting Equations (13)–(15) and (17) into Equation (29), respectively, give Equations (30)–(33), where the parameter C_3 is represented by Equation (34).

$$D_{\max} = \frac{n\sqrt{P_{\text{omax}} R_{\text{L}}}}{C_3} \tag{30}$$

$$D_{\max} = \frac{\sqrt{P_{\text{omax}} R_{\text{L}}}}{C_3/n + \sqrt{P_{\text{omax}} R_{\text{L}}}} = 1 - \frac{C_3/n}{C_3/n + \sqrt{P_{\text{omax}} R_{\text{L}}}} \tag{31}$$

$$D_{\max} = \frac{n\sqrt{P_{\text{omax}} R_{\text{L}}}}{2C_3} \tag{32}$$

$$V = C_3 \tag{33}$$

$$C_3 = C_2 V_{\text{oc}}[\text{lambertw}(\text{e} \times \frac{1+C_1}{C_1}) - 1] \tag{34}$$

According to Equation (34), it can be concluded that the value of C_3 is only related to the parameters of the PV cell itself (S and T). The simulation experiments revealed that P_{omax} is only affected by S and T and is independent of R_{L} and n. Therefore, only the values of C_3 and P_{omax} under different weather conditions are required to derive the relationship between $D_{\max}$ and R_{L}, n. This leads to the MPPT control of isolated PV systems to improve the efficiency. The C_3-S, C_3-T, P_{omax}-S and P_{omax}-T curves under different weather conditions were plotted using MATLAB, and by applying the curve-fitting method, Equations (35) and (36) can be obtained.

$$C_3 = 0.0057 \times S - 0.086 \times T + 26.15 \tag{35}$$

$$P_{\text{omax}} = \begin{cases} -5.5 \times 10^{-9} \times S^3 + 5.3 \times 10^{-5} \times S^2 + 0.17 \times S - 0.09 \times T - 1.45 & 0 \leq T \leq 40 \\ -5.5 \times 10^{-9} \times S^3 + 5.3 \times 10^{-5} \times S^2 + 0.17 \times S - 2.7 & -20 \leq T < 0 \end{cases} \tag{36}$$

According to Equations (35) and (36), C_3 and P_{omax} can be easily derived from the weather conditions. Meanwhile, in order to find the MCCs and improve the MPPT methodology of isolated PV systems, $D_{\max}$ can also be derived by combining the circuit parameters R_{L} and n.

Figure 4 shows the equivalent model of the isolated PV system at the MPP [12], where R_{iMPP}, V_{MPP} and I_{MPP} represent the values of R_{i}, V and I at the MPP in Figure 2, respectively.

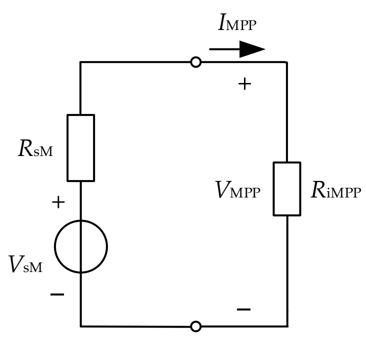

Figure 4. Isolated PV system with MPP linear model.

At the MPP, Equations (37) and (38) can be given by the circuit theorem [24].

$$R_{\text{iMPP}} = \frac{V_{\text{MPP}}}{I_{\text{MPP}}} \tag{37}$$

$$P_{\mathrm{omax}} = V_{\mathrm{MPP}} \times I_{\mathrm{MPP}} \tag{38}$$

Equations (33), (37) and (38) are combined to obtain Equation (39).

$$R_{\mathrm{iMPP}} = \frac{C_3^2}{P_{\mathrm{omax}}} \tag{39}$$

According to the maximum power transfer theorem [24], the isolated PV system can operate at the MPP when Equation (40) is satisfied.

$$R_{\mathrm{iMPP}} = R_{\mathrm{sM}} \tag{40}$$

Meanwhile, according to the circuit theorem [24], Equation (41) is satisfied.

$$V_{\mathrm{sM}} = 2C_3 \tag{41}$$

Using Equations (35), (36), (39) and (41), Equations (42) and (43) can be obtained.

$$R_{\mathrm{sM}}(S,T) = \frac{[C_3(S,T)]^2}{P_{\mathrm{omax}}(S,T)} \tag{42}$$

$$V_{\mathrm{sM}}(S,T) = 2C_3(S,T) \tag{43}$$

According to Equations (42) and (43), the MPP linear model of the PV cell can be built using MATLAB/Simulink. When the weather conditions change, R_{sM} is involved in the design of MPPT as the output signal of the model.

2.2. MCCs Based on the Engineering Model

The relationship between circuit parameters, weather conditions and control parameters has been derived in Section 2.1 when the output of the isolated DC/DC converter is a load resistor. This section continues to derive the MCCs for isolated PV systems with different topologies and outputs on the basis of the engineering cell model.

The circuit topologies of forward and flyback converters determine their D to satisfy Equation (44), those of half-bridge and push–pull converters determine their D to satisfy Equation (45), and that of the full-bridge converter determines its D to satisfy Equation (46) [23]. These three formulas are also the basis of the analysis of MCCs carried out in a later section. D_{max} represents D at the MPP.

$$0 < D_{\mathrm{max}} < 1 \tag{44}$$

$$0 < D_{\mathrm{max}} < 0.5 \tag{45}$$

$$0 < D_{\mathrm{max}} \leq 0.5 \tag{46}$$

Substituting Equation (30) into Equation (44), it can be seen that Equation (47) is satisfied. This is the R_{L} range in which the PV-Forward system can successfully track the MPP.

$$0 < R_{\mathrm{L}} < \frac{C_3^2}{n^2 P_{\mathrm{omax}}} \tag{47}$$

If the transformer ratio n is the object of study, Equation (47) can be replaced by Equation (48).

$$0 < n < \frac{C_3}{\sqrt{P_{\mathrm{omax}} R_{\mathrm{L}}}} \tag{48}$$

Similarly, the MCCs in the ideal case using the different PV systems are displayed in Table 1. These expressions are the prerequisites of successful MPPT control for isolated PV systems in the ideal case.

Table 1. Theoretical expressions of MCCs.

PV System	Range of the Output	Range of n
PV-Forward	$0 < R_L < \frac{C_3^2}{n^2 P_{omax}}$	$0 < n < \frac{C_3}{\sqrt{P_{omax} R_L}}$
PV-Flyback	$0 < R_L$	$0 < n$
PV-Half-bridge	$0 < R_L < \frac{C_3^2}{4n^2 P_{omax}}$	$0 < n < \frac{C_3}{2\sqrt{P_{omax} R_L}}$
PV-Full-bridge	$0 < R_L \leq \frac{C_3^2}{n^2 P_{omax}}$	$0 < n \leq \frac{C_3}{\sqrt{P_{omax} R_L}}$
PV-Forward-Dbus	$0 < V_{Dbus} < \frac{C_3}{n}$	$0 < n < \frac{C_3}{V_{Dbus}}$
PV-Flyback-Dbus	$0 < V_{Dbus}$	$0 < n$
PV-Half-bridge-Dbus	$0 < V_{Dbus} < \frac{C_3}{2n}$	$0 < n < \frac{C_3}{2V_{Dbus}}$
PV-Full-bridge-Dbus	$0 < V_{Dbus} \leq \frac{C_3}{n}$	$0 < n \leq \frac{C_3}{V_{Dbus}}$
PV-Forward-INV	$0 < R_L < \frac{M^2 C_3^2}{2n^2 P_{omax}}$	$0 < n < \frac{M C_3}{\sqrt{2 P_{omax} R_L}}$
PV-Flyback-INV	$0 < R_L$	$0 < n$
PV-Half-bridge-INV	$0 < R_L < \frac{M^2 C_3^2}{8n^2 P_{omax}}$	$0 < n < \frac{M C_3}{2\sqrt{2 P_{omax} R_L}}$
PV-Full-bridge-INV	$0 < R_L \leq \frac{M^2 C_3^2}{2n^2 P_{omax}}$	$0 < n \leq \frac{M C_3}{\sqrt{2 P_{omax} R_L}}$
PV-Forward-INV-Abus	$0 < V_{Abus} < \frac{C_3 M}{\sqrt{2} n}$	$0 < n < \frac{C_3 M}{\sqrt{2} V_{Abus}}$
PV-Flyback-INV-Abus	$0 < V_{Abus}$	$0 < n$
PV-Half-bridge-INV-Abus	$0 < V_{Abus} < \frac{C_3 M}{2\sqrt{2} n}$	$0 < n < \frac{C_3 M}{2\sqrt{2} V_{Abus}}$
PV-Full-bridge-INV-Abus	$0 < V_{Abus} \leq \frac{C_3 M}{\sqrt{2} n}$	$0 < n \leq \frac{C_3 M}{\sqrt{2} V_{Abus}}$

From the practical application point of view, the isolated PV system is a non-ideal circuit, and the expressions in Table 1 need to be improved. The duty cycle of the isolated DC/DC converter cannot be too small or too large due to the losses of the switching devices and the isolation transformer itself, the limitations on the switching device's opening and closing times and the through-current withstand voltage, the transmission delay of the controller and the PWM sampling delay. Therefore, in order to find the MCCs in practical applications, it is assumed that the minimum D of the forward and flyback converters is D_{L1}, while their maximum D is D_{U1}, and the minimum D of the half-bridge, full-bridge and push–pull converters is D_{L2}, while their maximum D is D_{U2}. At this point, the duty cycle ranges of the forward and flyback converters can be expressed by Equation (49), and the half-bridge, full-bridge and push–pull converter duty cycle ranges can be expressed by Equation (50).

$$D_{L1} \leq D_{max} \leq D_{U1} \tag{49}$$

$$D_{L2} \leq D_{max} \leq D_{U2} \tag{50}$$

Substituting Equation (30) into Equation (49), it can be seen that Equation (51) can be obtained. This is the R_L range in which the PV-Forward system can successfully track the MPP in practical applications.

$$\frac{D_{L1}^2 C_3^2}{n^2 P_{omax}} \leq R_L \leq \frac{D_{U1}^2 C_3^2}{n^2 P_{omax}} \tag{51}$$

If the transformer ratio n is the object of study, Equation (51) can be replaced by Equation (52).

$$\frac{D_{L1} C_3}{\sqrt{P_{omax} R_L}} \leq n \leq \frac{D_{U1} C_3}{\sqrt{P_{omax} R_L}} \tag{52}$$

Similarly, the MCCs of various isolated PV systems can be derived when the D limitation in a practical situation is considered, as shown in Table 2. These expressions are the prerequisites of successful MPPT control for isolated PV systems in practical applications.

Table 2. Practical expressions of MCCs.

PV System	Range of the Output	Range of n
PV-Forward	$\frac{D_{L1}^2 C_3^2}{n^2 P_{omax}} \le R_L \le \frac{D_{U1}^2 C_3^2}{n^2 P_{omax}}$	$\frac{D_{L1} C_3}{\sqrt{P_{omax} R_L}} \le n \le \frac{D_{U1} C_3}{\sqrt{P_{omax} R_L}}$
PV-Flyback	$\frac{D_{L1}^2 C_3^2}{n^2 (1-D_{L1})^2 P_{omax}} \le R_L \le \frac{D_{U1}^2 C_3^2}{n^2 (1-D_{U1})^2 P_{omax}}$	$\frac{D_{L1} C_3}{(1-D_{L1})\sqrt{P_{omax} R_L}} \le n \le \frac{D_{U1} C_3}{(1-D_{U1})\sqrt{P_{omax} R_L}}$
PV-Half-bridge	$\frac{D_{L2}^2 C_3^2}{n^2 P_{omax}} \le R_L \le \frac{D_{U2}^2 C_3^2}{n^2 P_{omax}}$	$\frac{D_{L2} C_3}{\sqrt{P_{omax} R_L}} \le n \le \frac{D_{U2} C_3}{\sqrt{P_{omax} R_L}}$
PV-Full-bridge	$\frac{4D_{L2}^2 C_3^2}{n^2 P_{omax}} \le R_L \le \frac{4D_{U2}^2 C_3^2}{n^2 P_{omax}}$	$\frac{2D_{L2} C_3}{\sqrt{P_{omax} R_L}} \le n \le \frac{2D_{U2} C_3}{\sqrt{P_{omax} R_L}}$
PV-Forward-Dbus	$\frac{C_3 D_{L1}}{n} \le V_{Dbus} \le \frac{C_3 D_{U1}}{n}$	$\frac{C_3 D_{L1}}{V_{Dbus}} \le n \le \frac{C_3 D_{U1}}{V_{Dbus}}$
PV-Flyback-Dbus	$\frac{C_3 D_{L1}}{n(1-D_{L1})} < V_{Dbus} \le \frac{C_3 D_{U1}}{n(1-D_{U1})}$	$\frac{C_3 D_{L1}}{V_{Dbus}(1-D_{L1})} < n \le \frac{C_3 D_{U1}}{V_{Dbus}(1-D_{U1})}$
PV-Half-bridge-Dbus	$\frac{C_3 D_{L2}}{n} \le V_{Dbus} \le \frac{C_3 D_{U2}}{n}$	$\frac{C_3 D_{L2}}{V_{Dbus}} \le n \le \frac{C_3 D_{U2}}{V_{Dbus}}$
PV-Full-bridge-Dbus	$\frac{2C_3 D_{L2}}{n} \le V_{Dbus} \le \frac{2C_3 D_{U2}}{n}$	$\frac{2C_3 D_{L2}}{V_{Dbus}} \le n \le \frac{2C_3 D_{U2}}{V_{Dbus}}$
PV-Forward-INV	$\frac{M^2 C_3^2 D_{L1}^2}{2n^2 P_{omax}} \le R_L \le \frac{M^2 C_3^2 D_{U1}^2}{2n^2 P_{omax}}$	$\frac{MD_{L1} C_3}{\sqrt{2P_{omax} R_L}} \le n \le \frac{MD_{U1} C_3}{\sqrt{2P_{omax} R_L}}$
PV-Flyback-INV	$\frac{M^2 C_3^2 D_{L1}^2}{2n^2 P_{omax}(1-D_{L1})^2} \le R_L \le \frac{M^2 C_3^2 D_{U1}^2}{2n^2 P_{omax}(1-D_{U1})^2}$	$\frac{MD_{L1} C_3}{(1-D_{L1})\sqrt{2P_{omax} R_L}} \le n \le \frac{MD_{U1} C_3}{(1-D_{U1})\sqrt{2P_{omax} R_L}}$
PV-Half-bridge-INV	$\frac{M^2 C_3^2 D_{L2}^2}{2n^2 P_{omax}} \le R_L \le \frac{M^2 C_3^2 D_{U2}^2}{2n^2 P_{omax}}$	$\frac{MD_{L2} C_3}{\sqrt{2P_{omax} R_L}} \le n \le \frac{MD_{U2} C_3}{\sqrt{2P_{omax} R_L}}$
PV-Full-bridge-INV	$\frac{2M^2 C_3^2 D_{L2}^2}{n^2 P_{omax}} \le R_L \le \frac{2M^2 C_3^2 D_{U2}^2}{n^2 P_{omax}}$	$\frac{\sqrt{2}MD_{L2} C_3}{\sqrt{P_{omax} R_L}} \le n \le \frac{\sqrt{2}MD_{U2} C_3}{\sqrt{P_{omax} R_L}}$
PV-Forward-INV-Abus	$\frac{C_3 MD_{L1}}{\sqrt{2}n} \le V_{Abus} \le \frac{C_3 MD_{U1}}{\sqrt{2}n}$	$\frac{C_3 MD_{L1}}{\sqrt{2}V_{Abus}} \le n \le \frac{C_3 MD_{U1}}{\sqrt{2}V_{Abus}}$
PV-Flyback-INV-Abus	$\frac{C_3 MD_{L1}}{\sqrt{2}n(1-D_{L1})} \le V_{Abus} \le \frac{C_3 MD_{U1}}{\sqrt{2}n(1-D_{U1})}$	$\frac{C_3 MD_{L1}}{\sqrt{2}V_{Abus}(1-D_{L1})} \le n \le \frac{C_3 MD_{U1}}{\sqrt{2}V_{Abus}(1-D_{U1})}$
PV-Half-bridge-INV-Abus	$\frac{C_3 MD_{L2}}{\sqrt{2}n} \le V_{Abus} \le \frac{C_3 MD_{U2}}{\sqrt{2}n}$	$\frac{C_3 MD_{L2}}{\sqrt{2}V_{Abus}} \le n \le \frac{C_3 MD_{U2}}{\sqrt{2}V_{Abus}}$
PV-Full-bridge-INV-Abus	$\frac{\sqrt{2}C_3 MD_{L2}}{n} \le V_{Abus} \le \frac{\sqrt{2}C_3 MD_{U2}}{n}$	$\frac{\sqrt{2}C_3 MD_{L2}}{V_{Abus}} \le n \le \frac{\sqrt{2}C_3 MD_{U2}}{V_{Abus}}$

2.3. MCCs Based on the MPP Linear Model

2.3.1. Expression of MCCs

The analysis in Section 2.2 has produced the ranges of circuit parameters for twenty isolated PV systems capable of MPPT control based on the engineering model. This section continues with an in-depth study of these circuit parameter ranges based on the MPP linear model. After the engineering model has been linearized by using the methodology in Section 2.1, the isolated PV system structure can be replaced by the system shown in Figure 5. The flyback converter is selected as an example, where V_{sM} and R_{sM} are quantities that vary with the weather conditions (S and T).

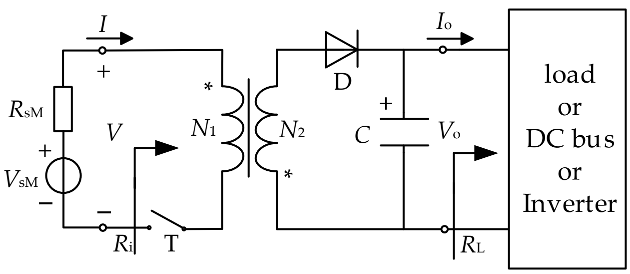

Figure 5. Isolated PV system based on MPP linear model. (* indicates the eponymous end of the induced electromotive force of the winding).

In order to find the MCCs in the ideal case, according to the maximum power transfer theorem, it can be seen that Equations (53) and (54) are satisfied when the PV system is operating at the MPP.

$$R_{\mathrm{i}} = R_{\mathrm{sM}} \tag{53}$$

$$V_{\mathrm{sM}} = 2V \tag{54}$$

The R_{i} of the PV-Forward system can be expressed by Equation (55), and R_{i} will vary with the different output devices and the transformations of isolated DC/DC converters.

$$R_{\mathrm{i}} = \frac{n^2 R_{\mathrm{L}}}{D^2} \tag{55}$$

The R_{i} of the PV-Forward-INV system can be expressed by Equation (56).

$$R_{\mathrm{i}} = \frac{2n^2 R_{\mathrm{L}}}{M^2 D^2} \tag{56}$$

Equation (56) reveals the mathematical relationship between the circuit parameters (R_{i}, R_{L} and n) and the control signals (D and M). On the basis of these expressions, the MCCs can be found.

When the output of the PV cell is connected to a resistor, Equation (55) is substituted into Equation (53), and then Equation (57) can be obtained.

$$D_{\max} = n\sqrt{\frac{R_{\mathrm{L}}}{R_{\mathrm{sM}}}} \tag{57}$$

Substituting Equation (56) into Equation (53), it can be seen that Equation (58) is satisfied. This is the R_{L} range in which the PV-Forward system can successfully track the MPP.

$$0 < R_{\mathrm{L}} < \frac{R_{\mathrm{sM}}}{n^2} \tag{58}$$

If the transformer ratio n is the object of study, Equation (58) can be replaced by Equation (59).

$$0 < n < \sqrt{\frac{R_{\mathrm{sM}}}{R_{\mathrm{L}}}} \tag{59}$$

Similarly, the MCCs of the different PV systems in the ideal case are displayed in Table 3. These expressions are the prerequisites of successful MPPT control for isolated PV systems in the ideal case.

Table 3 shows that under ideal conditions, an R_{L} or n value always exists in the PV-Flyback system to match the conditions for the use of the MPP linear model. Also, Table 3 shows that under ideal conditions, a V_{Dbus} or n value always exists in the PV-Flyback-Dbus system to match the use of the linear model. In contrast, for other PV systems, some constraints always exist. In addition, the use of inverters in isolated PV systems also affects the ranges of R_{L} and n. For the PV-Forward-INV, PV-Half-bridge-INV and PV-Full-bridge-INV systems, the presence of inverters narrows the ranges of R_{L} and n. Obviously, the expressions shown in Table 3 are the theoretical expressions of the MCCs, which can be used as the basis for designing the MPPT control process and proposing the MPPT control strategy under ideal conditions.

Table 3. Theoretical expressions of MCCs.

PV System	Range of the Output	Range of n
PV-Forward	$0 < R_{\mathrm{L}} < \frac{R_{\mathrm{sM}}}{n^2}$	$0 < n < \sqrt{\frac{R_{\mathrm{sM}}}{R_{\mathrm{L}}}}$
PV-Flyback	$0 < R_{\mathrm{L}}$	$0 < n$
PV-Half-bridge	$0 < R_{\mathrm{L}} < \frac{R_{\mathrm{sM}}}{4n^2}$	$0 < n < \frac{1}{2}\sqrt{\frac{R_{\mathrm{sM}}}{R_{\mathrm{L}}}}$
PV-Full-bridge	$0 < R_{\mathrm{L}} \leq \frac{R_{\mathrm{sM}}}{n^2}$	$0 < n \leq \sqrt{\frac{R_{\mathrm{sM}}}{R_{\mathrm{L}}}}$
PV-Forward-Dbus	$0 < V_{\mathrm{Dbus}} < \frac{V_{\mathrm{sM}}}{2n}$	$0 < n < \frac{V_{\mathrm{sM}}}{2V_{\mathrm{Dbus}}}$
PV-Flyback-Dbus	$0 < V_{\mathrm{Dbus}}$	$0 < n$
PV-Half-bridge-Dbus	$0 < V_{\mathrm{Dbus}} \leq \frac{V_{\mathrm{sM}}}{4n}$	$0 < n < \frac{V_{\mathrm{sM}}}{4V_{\mathrm{Dbus}}}$
PV-Full-bridge-Dbus	$0 < V_{\mathrm{Dbus}} \leq \frac{V_{\mathrm{sM}}}{2n}$	$0 < n \leq \frac{V_{\mathrm{sM}}}{2V_{\mathrm{Dbus}}}$
PV-Forward-INV	$0 < R_{\mathrm{L}} < \frac{M^2 R_{\mathrm{sM}}}{2n^2}$	$0 < n < M\sqrt{\frac{R_{\mathrm{sM}}}{2R_{\mathrm{L}}}}$
PV-Flyback-INV	$0 < R_{\mathrm{L}}$	$0 < n$
PV-Half-bridge-INV	$0 < R_{\mathrm{L}} < \frac{M^2 R_{\mathrm{sM}}}{8n^2}$	$0 < n < \frac{M}{2}\sqrt{\frac{R_{\mathrm{sM}}}{2R_{\mathrm{L}}}}$
PV-Full-bridge-INV	$0 < R_{\mathrm{L}} \leq \frac{M^2 R_{\mathrm{sM}}}{2n^2}$	$0 < n \leq M\sqrt{\frac{R_{\mathrm{sM}}}{2R_{\mathrm{L}}}}$

From the practical application point of view, the isolated PV system is a non-ideal circuit, and the expressions in Table 3 need to be improved. The duty cycle of the isolated DC/DC converter cannot be too small or too large. Therefore, in order to find the range of circuit parameters in practical applications, the duty cycle ranges of the forward, flyback, half-bridge, full-bridge and push–pull converters are expressed by Equations (49) and (50).

Substituting Equation (57) into Equation (49), it can be seen that Equation (60) is satisfied. This is the R_{L} range in which MPPT control can be successfully realized in practical applications for the PV-Forward system.

$$\frac{D_{\mathrm{L1}}^2 R_{\mathrm{sM}}}{n^2} \leq R_L \leq \frac{D_{\mathrm{U1}}^2 R_{\mathrm{sM}}}{n^2} \tag{60}$$

If the transformer ratio n is the object of study, Equation (60) can be replaced by Equation (61).

$$D_{\mathrm{L1}}\sqrt{\frac{R_{\mathrm{sM}}}{R_{\mathrm{L}}}} \leq n \leq D_{\mathrm{U1}}\sqrt{\frac{R_{\mathrm{sM}}}{R_{\mathrm{L}}}} \tag{61}$$

Similarly, the ranges of circuit parameters in which various isolated PV systems are capable of successfully realizing MPPT are shown in Table 4, when considering the limited range of D in practical situations. These expressions are the prerequisites of successful MPPT control for isolated PV systems in practical situations.

Table 4 shows significantly smaller ranges for R_{L} and V_{Dbus} when compared with those in Table 3. Unlike the ideal case, the PV-Flyback, PV-Flyback-Dbus and PV-Flyback-INV systems have certain constraints in practical applications. Obviously, the expressions in Table 4 provide a theoretical basis for isolated PV systems on the basis of the MPP linear model in practical applications.

2.3.2. Range of MCCs

The ranges of V_{sM} and R_{sM} have been derived for changing weather conditions. Therefore, the extreme values of MCCs for practical applications are shown in Table 5. It can be seen that the maximum range of R_{L} (or V_{Dbus}) is necessary for each PV system to be modeled with the MPP linear cell. By contrast, the minimum range of R_{L} (or V_{Dbus}) is a sufficient condition for every PV system to use the MPP linear model. Similarly, the maximum and minimum ranges of the variable ratio n can be derived analogously.

Table 4. Practical expressions of MCCs.

PV System	Range of the Output	Range of n
PV-Forward	$\frac{D_{L1}^2 R_{sM}}{n^2} \le R_L \le \frac{D_{U1}^2 R_{sM}}{n^2}$	$D_{L1}\sqrt{\frac{R_{sM}}{R_L}} \le n \le D_{U1}\sqrt{\frac{R_{sM}}{R_L}}$
PV-Flyback	$\frac{D_{L1}^2 R_{sM}}{n^2(1-D_{L1})^2} \le R_L \le \frac{D_{U1}^2 R_{sM}}{n^2(1-D_{U1})^2}$	$\frac{D_{L1}}{(1-D_{L1})}\sqrt{\frac{R_{sM}}{R_L}} \le n \le \frac{D_{U1}}{(1-D_{U1})}\sqrt{\frac{R_{sM}}{R_L}}$
PV-Half-bridge	$\frac{D_{L2}^2 R_{sM}}{n^2} \le R_L \le \frac{D_{U2}^2 R_{sM}}{n^2}$	$D_{L2}\sqrt{\frac{R_{sM}}{R_L}} \le n \le D_{U2}\sqrt{\frac{R_{sM}}{R_L}}$
PV-Full-bridge	$\frac{4D_{L2}^2 R_{sM}}{n^2} \le R_L \le \frac{4D_{U2}^2 R_{sM}}{n^2}$	$2D_{L2}\sqrt{\frac{R_{sM}}{R_L}} \le n \le 2D_{U2}\sqrt{\frac{R_{sM}}{R_L}}$
PV-Forward-Dbus	$\frac{D_{L1} V_{sM}}{2n} \le V_{Dbus} \le \frac{D_{U1} V_{sM}}{2n}$	$\frac{D_{L1} V_{sM}}{2V_{Dbus}} \le n \le \frac{D_{U1} V_{sM}}{2V_{Dbus}}$
PV-Flyback-Dbus	$\frac{D_{L1} V_{sM}}{2n(1-D_{L1})} < V_{Dbus} \le \frac{D_{U1} V_{sM}}{2n(1-D_{U1})}$	$\frac{D_{L1} V_{sM}}{2V_{Dbus}(1-D_{L1})} < n \le \frac{D_{U1} V_{sM}}{2V_{Dbus}(1-D_{U1})}$
PV-Half-bridge-Dbus	$\frac{D_{L2} V_{sM}}{2n} \le V_{Dbus} \le \frac{D_{U2} V_{sM}}{2n}$	$\frac{D_{L2} V_{sM}}{2V_{Dbus}} \le n \le \frac{D_{U2} V_{sM}}{2V_{Dbus}}$
PV-Full-bridge-Dbus	$\frac{D_{L2} V_{sM}}{n} \le V_{Dbus} \le \frac{D_{U2} V_{sM}}{n}$	$\frac{D_{L2} V_{sM}}{V_{Dbus}} \le n \le \frac{D_{U2} V_{sM}}{V_{Dbus}}$
PV-Forward-INV	$\frac{D_{L1}^2 M^2 R_{sM}}{2n^2} \le R_L \le \frac{D_{U1}^2 M^2 R_{sM}}{2n^2}$	$MD_{L1}\sqrt{\frac{R_{sM}}{2R_L}} \le n \le MD_{U1}\sqrt{\frac{R_{sM}}{2R_L}}$
PV-Flyback-INV	$\frac{D_{L1}^2 M^2 R_{sM}}{2n^2(1-D_{L1})^2} \le R_L \le \frac{D_{U1}^2 M^2 R_{sM}}{2n^2(1-D_{U1})^2}$	$\frac{MD_{L1}}{(1-D_{L1})}\sqrt{\frac{R_{sM}}{2R_L}} \le n \le \frac{MD_{U1}}{(1-D_{U1})}\sqrt{\frac{R_{sM}}{2R_L}}$
PV-Half-bridge-INV	$\frac{D_{L2}^2 M^2 R_{sM}}{2n^2} \le R_L \le \frac{D_{U2}^2 M^2 R_{sM}}{2n^2}$	$MD_{L2}\sqrt{\frac{R_{sM}}{2R_L}} \le n \le MD_{U2}\sqrt{\frac{R_{sM}}{2R_L}}$
PV-Full-bridge-INV	$\frac{2D_{L2}^2 M^2 R_{sM}}{n^2} \le R_L \le \frac{2D_{U2}^2 M^2 R_{sM}}{n^2}$	$MD_{L2}\sqrt{\frac{2R_{sM}}{R_L}} \le n \le MD_{U2}\sqrt{\frac{2R_{sM}}{R_L}}$

Table 5. Ranges of MCCs.

PV System	Maximum Range	Minimum Range
PV-Forward	$\frac{D_{L1}^2 R_{sMmin}}{n^2} \le R_L \le \frac{D_{U1}^2 R_{sMmax}}{n^2}$	$\frac{D_{L1}^2 R_{sMmax}}{n^2} \le R_L \le \frac{D_{U1}^2 R_{sMmin}}{n^2}$
PV-Flyback	$\frac{D_{L1}^2 R_{sMmin}}{n^2(1-D_{L1})^2} \le R_L \le \frac{D_{U1}^2 R_{sMmax}}{n^2(1-D_{U1})^2}$	$\frac{D_{L1}^2 R_{sMmax}}{n^2(1-D_{L1})^2} \le R_L \le \frac{D_{U1}^2 R_{sMmin}}{n^2(1-D_{U1})^2}$
PV-Half-bridge	$\frac{D_{L2}^2 R_{sMmin}}{n^2} \le R_L \le \frac{D_{U2}^2 R_{sMmax}}{n^2}$	$\frac{D_{L2}^2 R_{sMmax}}{n^2} \le R_L \le \frac{D_{U2}^2 R_{sMmin}}{n^2}$
PV-Full-bridge	$\frac{4D_{L2}^2 R_{sMmin}}{n^2} \le R_L \le \frac{4D_{U2}^2 R_{sMmax}}{n^2}$	$\frac{4D_{L2}^2 R_{sMmax}}{n^2} \le R_L \le \frac{4D_{U2}^2 R_{sMmin}}{n^2}$
PV-Forward-Dbus	$\frac{D_{L1} V_{sMmin}}{2n} \le V_{Dbus} \le \frac{D_{U1} V_{sMmax}}{2n}$	$\frac{D_{L1} V_{sMmax}}{2n} \le V_{Dbus} \le \frac{D_{U1} V_{sMmin}}{2n}$
PV-Flyback-Dbus	$\frac{D_{L1} V_{sMmin}}{2n(1-D_{L1})} < V_{Dbus} \le \frac{D_{U1} V_{sMmax}}{2n(1-D_{U1})}$	$\frac{D_{L1} V_{sMmax}}{2n(1-D_{L1})} < V_{Dbus} \le \frac{D_{U1} V_{sMmin}}{2n(1-D_{U1})}$
PV-Half-bridge-Dbus	$\frac{D_{L2} V_{sMmin}}{2n} \le V_{Dbus} \le \frac{D_{U2} V_{sMmax}}{2n}$	$\frac{D_{L2} V_{sMmax}}{2n} \le V_{Dbus} \le \frac{D_{U2} V_{sMmin}}{2n}$
PV-Full-bridge-Dbus	$\frac{D_{L2} V_{sMmin}}{n} \le V_{Dbus} \le \frac{D_{U2} V_{sMmax}}{n}$	$\frac{D_{L2} V_{sMmax}}{n} \le V_{Dbus} \le \frac{D_{U2} V_{sMmin}}{n}$
PV-Forward-INV	$\frac{D_{L1}^2 M^2 R_{sMmin}}{2n^2} \le R_L \le \frac{D_{U1}^2 M^2 R_{sMmax}}{2n^2}$	$\frac{D_{L1}^2 M^2 R_{sMmax}}{2n^2} \le R_L \le \frac{D_{U1}^2 M^2 R_{sMmin}}{2n^2}$
PV-Flyback-INV	$\frac{D_{L1}^2 M^2 R_{sMmin}}{2n^2(1-D_{L1})^2} \le R_L \le \frac{D_{U1}^2 M^2 R_{sMmax}}{2n^2(1-D_{U1})^2}$	$\frac{D_{L1}^2 M^2 R_{sMmax}}{2n^2(1-D_{L1})^2} \le R_L \le \frac{D_{U1}^2 M^2 R_{sMmin}}{2n^2(1-D_{U1})^2}$
PV-Half-bridge-INV	$\frac{D_{L2}^2 M^2 R_{sMmin}}{2n^2} \le R_L \le \frac{D_{U2}^2 M^2 R_{sMmax}}{2n^2}$	$\frac{D_{L2}^2 M^2 R_{sMmax}}{2n^2} \le R_L \le \frac{D_{U2}^2 M^2 R_{sMmin}}{2n^2}$
PV-Full-bridge-INV	$\frac{2D_{L2}^2 M^2 R_{sMmin}}{n^2} \le R_L \le \frac{2D_{U2}^2 M^2 R_{sMmax}}{n^2}$	$\frac{2D_{L2}^2 M^2 R_{sMmax}}{n^2} \le R_L \le \frac{2D_{U2}^2 M^2 R_{sMmin}}{n^2}$

In practical applications, Tables 3–5 are a good guide for the circuit design, theoretical derivation and product selection of isolated PV systems. On the one hand, it is complicated to adjust the output under changing weather conditions. In order to realize MPPT control, they can be used to select the types of isolated DC/DC converters and circuit components. On the other hand, they can also be used as a basis for the study of MPPT methods. Meanwhile, they can be used to estimate the MPPT effect based on the recorded historical data of S and T in the application area. In addition, the results shown in Table 5 can provide a theoretical basis when the overall linearized model of the isolated PV system is investigated.

2.4. Two New MPPT Methods Based on MPP Linear Modeling

Two new MPPT methods based on the MPP linear model are proposed. Here, the PV-Flyback and PV-Flyback-Dbus systems are used as examples.

2.4.1. MPPT Method for PV Systems with Resistive Output (RMPPT)

Substituting Equations (4)–(6), (8) and (42) into (53), Equation (62) is satisfied. It relates $D_{\max}$ to the weather conditions (S and T) and the circuit parameters (R_L and n) when the PV-Flyback system operates at the MPP.

$$D_{\max} = \frac{n\sqrt{R_L}}{\sqrt{R_{sM}(S,T)} + n\sqrt{R_L}} \tag{62}$$

According to Equation (62), it can be seen that RMPPT can be used when R_L and n are measured or known. Equation (62) is the theoretical basis of RMPPT, which can be described as follows: by measuring or knowing S and T as well as R_L and n, the duty cycle $D_{\max}$ at the MPP for the isolated PV system can be calculated, and the microcontroller or chip can realize MPPT control by controlling $D = D_{\max}$.

The structure of the isolated PV system using RMPPT is shown in Figure 6. As can be seen in Figure 6, the $D_{\max}$ value of the PV system when it is located at the MPP attachment can be simply calculated by using a microcontroller or chip to measure or know the weather parameters (S and T) and the circuit parameters (n, V_o and I_o), calculating the load resistor R_L and then substituting these parameters into Equation (62). When the input is a PV array, the cost of the sensor can be reduced by sharing the irradiance sensor if S is uniform in a certain area. Also, the cost of voltage sampling and current sampling can be reduced if R_L is essentially the same for each PV system. It can be seen that the implementation of RMPPT requires only a simple process with low computational complexity, which can greatly reduce the hardware cost and program design of an isolated PV system.

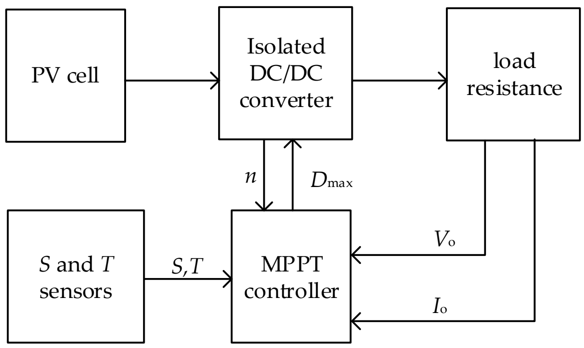

Figure 6. Isolated PV system structure of RMPPT.

2.4.2. MPPT Method with Output as DC Bus (BMPPT)

Substituting Equations (8), (16), (43) into (54), Equation (63) can be obtained. It relates $D_{\max}$ to the weather conditions (S and T) and the circuit parameters (V_{Dbus} and n) when the PV-Flyback-Dbus system operates at MPP.

$$D_{\max} = \frac{2nV_{Dbus}}{V_{sM}(S,T) + 2nV_{Dbus}} \tag{63}$$

According to Equation (63), it can be seen that when V_{Dbus} and n can be measured or known, BMPPT can be used. Equation (63) is the theoretical basis of BMPPT, which can be described as follows: From the measured or known S and T, as well as V_{Dbus} and n, the duty cycle at the MPP $D_{\max}$ of the isolated PV system can be calculated. Then, the microcontroller or chip makes the duty cycle of the PWM wave equal to $D_{\max}$, thereby achieving MPPT control. In contrast to RMPPT, BMPPT need not collect the output current. Eliminating the current-sampling device from the hardware design reduces the design difficulty and cost of the PV system and also reduces the current-sampling program designed for the software. When the output is a DC bus, BMPPT has an obvious advantage.

The structure of the isolated PV system using BMPPT is shown in Figure 7. As can be seen in Figure 7, the value of $D_{\max}$ for a PV system located at the MPP attachment can be simply calculated by using a microcontroller or chip to measure or know the weather conditions (S and T) and the circuit parameters (n and V_{Dbus}) and then substituting these parameters into Equation (63). Similarly, in the case of multiple PV arrays at the input, the cost of the sensors can be reduced by sharing irradiance sensors if S is uniform in a certain area. At the same time, multiple PV cells simplify the design of voltage-sampling circuits and reduce hardware and software costs by sharing a common set of DC buses.

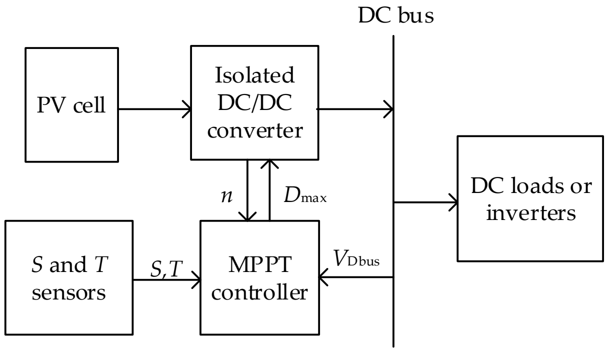

Figure 7. Isolated PV system structure of BMPPT.

3. Results

3.1. Simulation Verification of MCCs Based on the Engineering Model

In Table 2, it can be seen that the MCCs for PV systems with forward, half-bridge, full-bridge and push–pull converters are similar, as are the MCCs for PV systems with and without inverters. In this section, only the PV-Flyback, PV-Full-bridge, PV-Flyback-Dbus and PV-Full-bridge-Dbus systems are verified, and other PV systems with different structures can be verified analogously. In order to verify the accuracy of Table 2, some simulation experiments were carried out for PV systems with a flyback converter and full-bridge converter at STC with n = 1/10 or R_{L} = 5 Ω or V_{Dbus} = 500 V for three cases, respectively. The experimental results are shown in Figure 8. The four factory parameter settings of this PV cell model are the same as in the first PV cell (1Soltech 1STH-215-P) of the PV array module in MATLAB/Simulink, which are I_{sc} = 7.84 A, V_{oc} = 36.3 V, I_{m} = 7.35 A and V_{m} = 29 V, respectively.

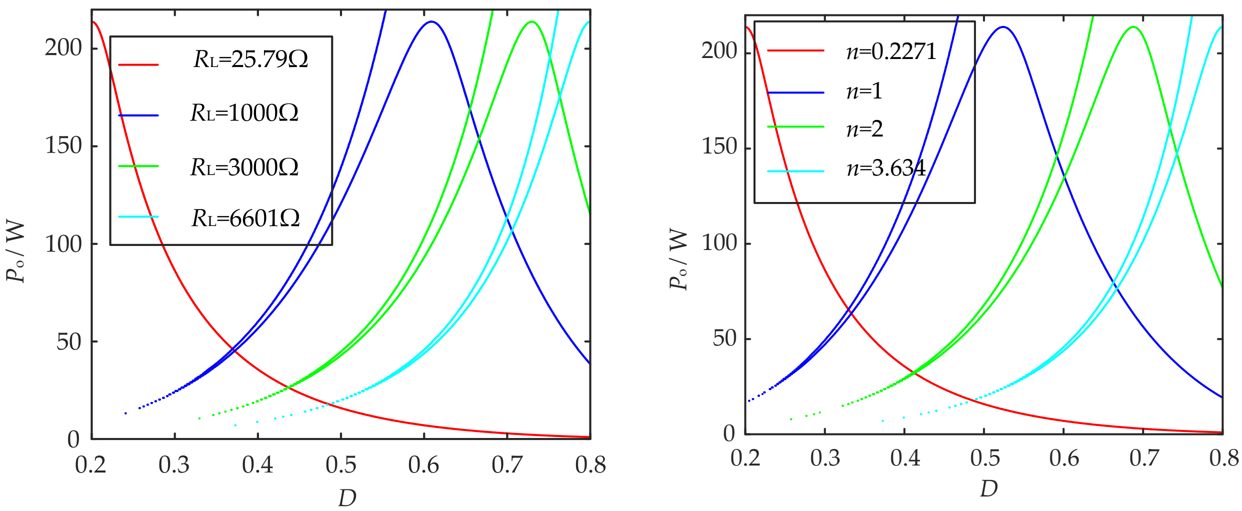

(**a**) (**b**)

Figure 8. *Cont.*

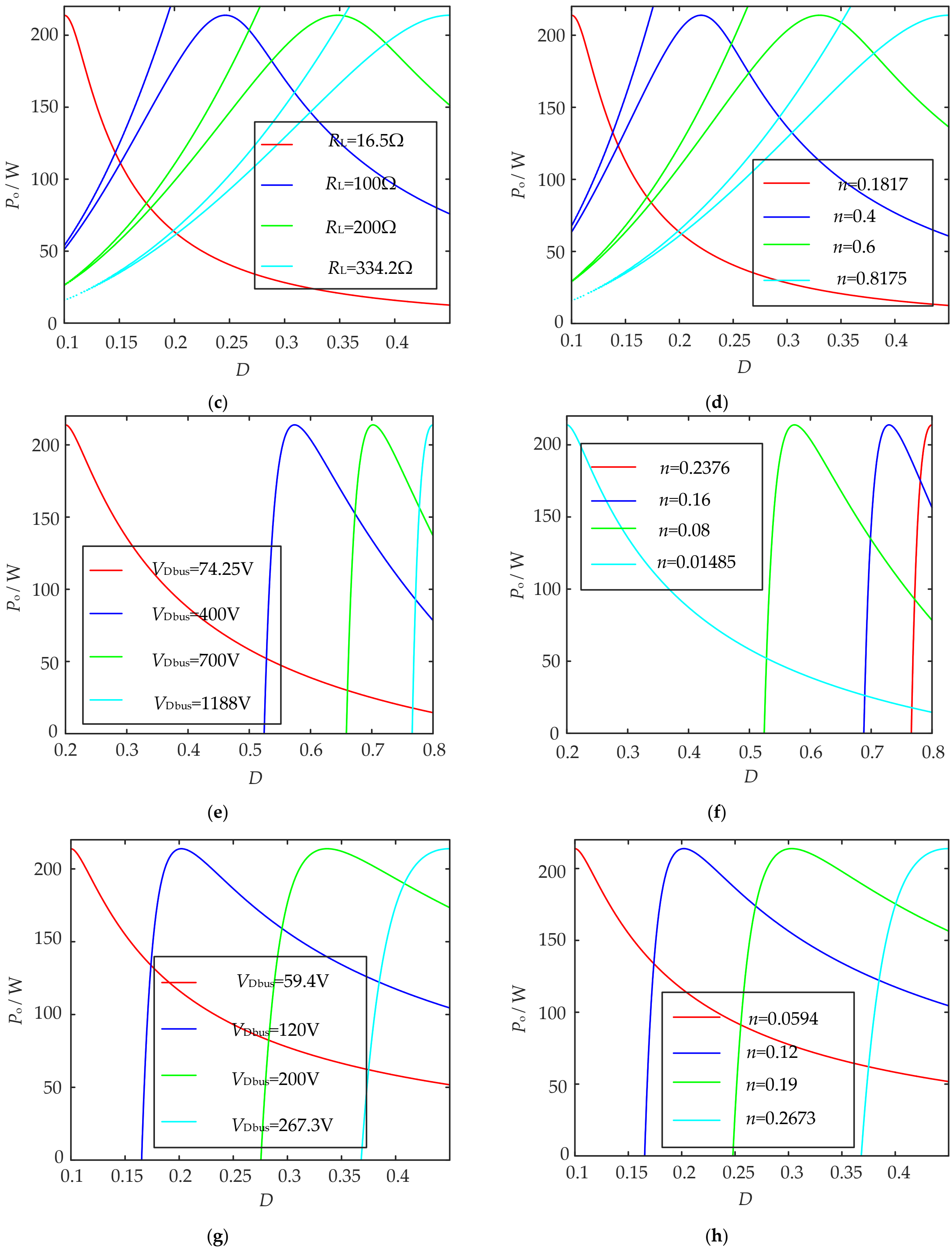

Figure 8. P_o-D curves of the different outputs and n. (**a**) P_o-D curves of PV-Flyback system for different R_L; (**b**) P_o-D curves of PV-Flyback system for different n; (**c**) P_o-D curves of PV-Full-bridge system for different R_L; (**d**) P_o-D curves of PV-Full-bridge system for different n; (**e**) P_o-D curves of PV-Flyback-Dbus for different V_{Dbus}; (**f**) P_o-D curves of PV-Flyback-Dbus for different n; (**g**) P_o-D curves of PV-Full-bridge-Dbus for different V_{Dbus}; (**h**) P_o-D curves of PV-Full-bridge-Dbus for different n.

Assume that D_{L1}, D_{U1}, D_{L2} and D_{U2} are taken as 0.2, 0.8, 0.1 and 0.45, respectively, that R_L = 5 Ω or V_{Dbus} = 500 V for the study of the range of n, and that n = 0.1 for the study of the range of R_L or V_{Dbus}. The calculated maximum and minimum values of the circuit parameter range for a PV system with a forward converter and a full-bridge converter capable of successful MPPT are shown in Table 6, where R_{Lmax} and R_{Lmin} denote the maximum and minimum values of R_L, respectively, n_{max} and n_{min} denote the maximum and minimum values of n, respectively, and V_{Dmax} and V_{Dmin} denote the maximum and minimum values of $V_{Dbus,}$ respectively. These data are compared with Figure 8 to analyze the reasonableness and accuracy of the MCCs.

Table 6. The extreme values of MCCs.

PV System	R_{Lmin} or V_{Dmin}	R_{Lmax} or V_{Dmax}	n_{min}	n_{max}
PV-Flyback	25.79 Ω	6601 Ω	0.2271	3.634
PV-Full-bridge	16.5 Ω	334.2 Ω	0.1817	0.8175
PV-Flyback-Dbus	74.25 V	1188 V	0.01485	0.2376
PV-Full-bridge-Dbus	59.4 V	267.3 V	0.0594	0.2673

According to Figure 8a,b,e,f, for the PV-Flyback and PV-Flyback-Dbus systems, when n is certain and $R_L = R_{Lmin}$ or $V_{Dbus} = V_{Dmin}$ is satisfied, the MPP is reached exactly at $D = D_{L1}$. When $R_L = R_{Lmax}$ or $V_{Dbus} = V_{Dmax}$ is satisfied, the MPP is reached exactly at $D = D_{U1}$. When R_L or V_{Dbus} is certain and $n = n_{min}$ is satisfied, the MPP is reached exactly at $D = D_{L1}$. When $n = n_{max}$, the MPP is reached exactly at $D = D_{U1}$.

In Figure 8c,d,g,h, it can be seen that, for the PV-Full-bridge and PV-Full-bridge-Dbus systems, the MPP is reached exactly at $D = D_{L2}$ when n is certain and $R_L = R_{Lmin}$ or $V_{Dbus} = V_{Dmin}$ is satisfied. When $R_L = R_{Lmax}$ or $V_{Dbus} = V_{Dmax}$ is satisfied, the MPP is reached exactly at $D = D_{U2}$. When R_L or V_{Dbus} is certain and $n = n_{min}$ is satisfied, the MPP is reached exactly at $D = D_{L2}$. When $n = n_{max}$ is satisfied, the MPP is reached exactly at $D = D_{U2}$.

In Table 6, it can be seen that the range of MCCs for the PV-Flyback and PV-Flyback-Dbus systems is much larger than that of the PV-Full-bridge and PV-Full-bridge-Dbus systems. However, in the small-load and low-variable-ratio segments, the range of MCCs for the PV-Full-bridge and PV-Full-bridge-Dbus systems is slightly larger than that for the PV-Flyback and PV-Flyback-Dbus PV systems.

In conclusion, according to Figure 8, the MCCs shown in Table 2 are accurate in practical applications when the duty cycle constraints of isolated DC/DC converters are considered.

Obviously, the MCCs of PV systems are influenced by the changing irradiance and temperature. Therefore, in the research and application of PV systems, we can judge the effect of MPPT control and estimate the range of its circuit parameters according to local historical meteorological data.

3.2. Simulation Verification of MCCs Based on MPP Linear Model

3.2.1. Accuracy Verification of MCCs

Table 7 shows the four weather conditions of the PV system, and simulation experiments were conducted for the MCCs. Meanwhile, the results in Tables 3–5 and other weather conditions can be verified analogously.

Table 7. Simulated weather parameters of PV system.

Weather Conditions	(a)	(b)	(c)	(d)
S (W/m^2)	1300	850	550	350
T (°C)	40	25	20	15

When the output of the PV system is resistive, D_{L1}, D_{U1}, D_{L2} and D_{U2} are taken as 0.2, 0.8, 0.1 and 0.45, respectively, and R_L is equal to 0.5 Ω. The simulation results are shown in Figure 9. Figure 9 compares the curves of D_{max} variation with n for the PV-Forward, PV-Flyback, PV-Half-bridge and PV-Full-bridge systems under four weather conditions. Meanwhile, the MCCs in Table 4 are calculated, and the results are shown in Table 8. They can verify the accuracy of the simulation results in Figure 9 and Table 4.

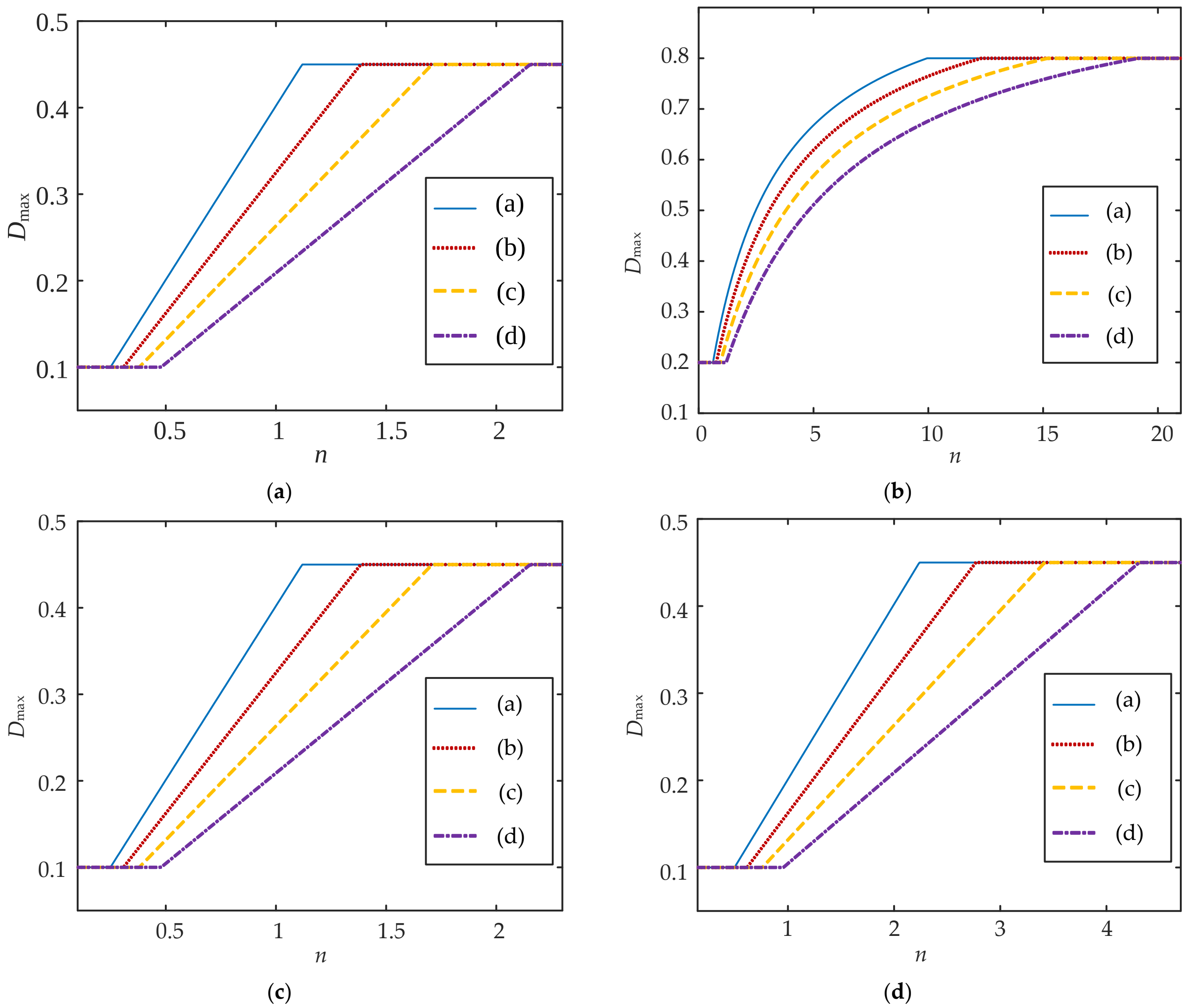

Figure 9. P_o-D curves of different PV systems. (**a**) D_{max}-n curves of PV-Forward system; (**b**) D_{max}-n curves of PV-Flyback system; (**c**) D_{max}-n curves of PV-Half-bridge system; (**d**) D_{max}-n curves of PV-Full-bridge system.

Table 8. Calculated values of MCCs.

Weather Conditions	(a)	(b)	(c)	(d)
PV-Forward	0.497	0.615	0.760	0.957
	1.989	2.462	3.038	3.829
PV-Flyback	0.622	0.769	0.949	1.197
	9.947	12.31	15.19	19.15
PV-Half-bridge	0.249	0.308	0.380	0.479
	1.119	1.385	1.709	2.154
PV-Full-bridge	0.497	0.615	0.760	0.957
	2.238	2.770	3.418	4.308

In Figure 9a, it can be seen that, for the PV-Forward system, $D_{\max}$ remains at 0.2 when $n < D_{L1}\sqrt{R_{sM}}/\sqrt{R_L}$ and 0.8 when $n > D_{U1}\sqrt{R_{sM}}/\sqrt{R_L}$, which implies that the MPP does not exist outside the range of n, and the MPP linear model cannot be used. In Figure 9b, it can be seen that, for the PV-Flyback system, $D_{\max}$ stays at 0.2 when $n < D_{L1}\sqrt{R_{sM}}/[\sqrt{R_L}(1-D_{L1})]$, while when $n > D_{U1}\sqrt{R_{sM}}/[\sqrt{R_L}(1-D_{U1})]$, Dmax stays at 0.8, which means that the MPP does not exist outside the range of n, and the MPP linear model cannot be used. In Figure 9c, it can be seen that, for the PV-Half-bridge system, $D_{\min}$ stays at 0.1 when $n < D_{L2}\sqrt{R_{sM}}/\sqrt{R_L}$, while $D_{\max}$ stays at 0.45 when $n > D_{U2}\sqrt{R_{sM}}/\sqrt{R_L}$, which implies that the MPP does not exist outside of the range of n, and the MPP linear model cannot be used. In Figure 9d, it can be seen that the PV-Full-bridge system maintains $D_{\min}$ at 0.1 when $n < 2D_{L2}\sqrt{R_{sM}}/\sqrt{R_L}$, while $D_{\max}$ remains at 0.45 under the condition of $n > 2D_{U2}\sqrt{R_{sM}}/\sqrt{R_L}$, which implies that the MPP does not exist outside the range of n, and the MPP linear model cannot be used.

Comparing Figure 9, the $D_{\max}$ of the PV system varies with n when n is within the MCCs. In this case, the MPP always exists, and the MPP linear model can be used for these four PV systems. The simulation results shown in Figure 9 are consistent with the corresponding data in Table 8, whereas the $D_{\max}$-n curves of PV systems under different weather conditions differ significantly. Therefore, it can be concluded that the practical expressions of MCCs for various isolated PV systems in Table 4 are accurate for the PV-Forward, PV-Flyback, PV-Half-bridge and PV-Full-bridge systems.

3.2.2. Comparison of MCCs

The fifteen PV systems studied in this section can be applied under a wide range of practical requirements. However, the choice of the right PV system is complex. Therefore, it is essential to compare their MCCs. Here, it is assumed that the values of D_{L1}, D_{L2}, D_{U1}, D_{U2}, n, R_L and V_{Dbus} are the same as in Section 3.2.1. In this case, Table 9 shows the calculated values according to Table 5.

Table 9. Calculated values of MCCs.

PV System	Calculated MCC Values	
PV-Forward	$0.28\sqrt{R_{sM}} \leq n \leq 1.13\sqrt{R_{sM}}$	$4R_{sM} \leq R_L \leq 64R_{sM}$
PV-Flyback	$0.35\sqrt{R_{sM}} \leq n \leq 5.66\sqrt{R_{sM}}$	$6.25R_{sM} \leq R_L \leq 1600R_{sM}$
PV-Half-bridge	$0.14\sqrt{R_{sM}} \leq n \leq 0.636\sqrt{R_{sM}}$	$R_{sM} \leq R_L < 20.25R_{sM}$
PV-Full-bridge	$0.28\sqrt{R_{sM}} \leq n \leq 1.272\sqrt{R_{sM}}$	$4R_{sM} \leq R_L < 81R_{sM}$
PV-Forward-Dbus	$0.01V_{sM} \leq n \leq 0.04V_{sM}$	$V_{sM} \leq V_{Dbus} \leq 4V_{sM}$
PV-Flyback-Dbus	$0.013V_{sM} \leq n \leq 0.2V_{sM}$	$1.25V_{sM} \leq V_{Dbus} \leq 20V_{sM}$
PV-Half-bridge-Dbus	$0.005V_{sM} \leq n \leq 0.02V_{sM}$	$0.5V_{sM} \leq V_{Dbus} < 2.25V_{sM}$
PV-Full-bridge-Dbus	$0.01V_{sM} \leq n \leq 0.045V_{sM}$	$V_{sM} \leq V_{Dbus} \leq 4.5\mathrm{V}_{sM}$
PV-Forward-INV	$0.16\sqrt{R_{sM}} \leq n \leq 0.64\sqrt{R_{sM}}$	$1.28R_{sM} \leq R_L \leq 20.48R_{sM}$
PV-Flyback-INV	$0.2\sqrt{R_{sM}} \leq n \leq 3.2\sqrt{R_{sM}}$	$2R_{sM} \leq R_L \leq 512R_{sM}$
PV-Half-bridge-INV	$0.08\sqrt{R_{sM}} \leq n \leq 0.36\sqrt{R_{sM}}$	$0.32R_{sM} \leq R_L < 6.48R_{sM}$
PV-Full-bridge-INV	$0.16\sqrt{R_{sM}} \leq n \leq 0.72\sqrt{R_{sM}}$	$1.28R_{sM} \leq R_L < 25.92R_{sM}$

Some simulations based on Table 9 were performed to further analyze the MCCs. The simulation results are shown in Figure 10. In Figure 10, R_{LminFD} and R_{LmaxHB} denote the maximum and minimum values of R_L for the PV-Forward system and PV-Half-bridge system, respectively. Other circuit parameter boundaries are also presented in Figure 10.

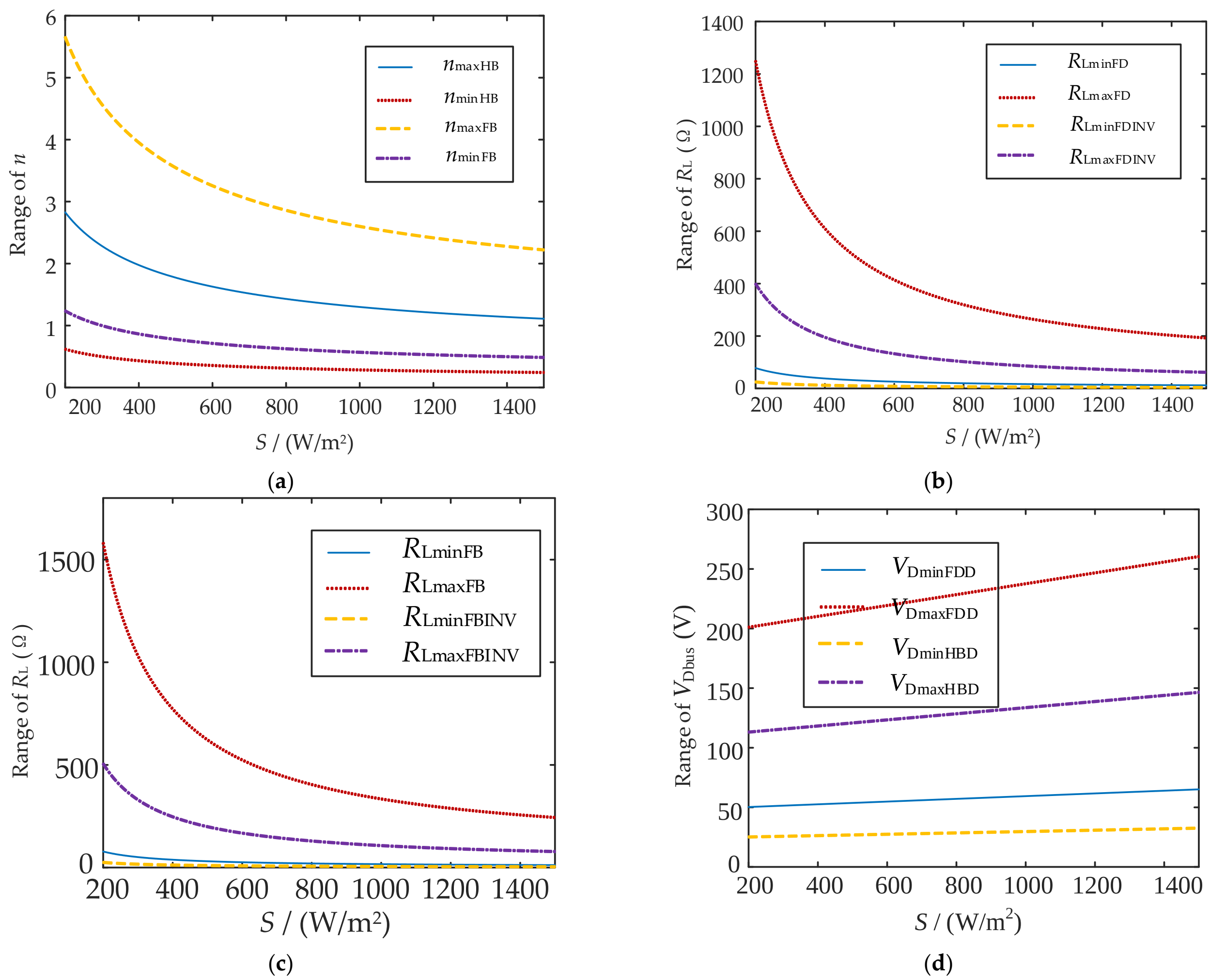

Figure 10. Comparison of curves of MCCs. (**a**) PV-Half-bridge compared with PV-Full-bridge system; (**b**) PV-Forward compared with PV-Forward-INV system; (**c**) PV-Full-bridge compared with PV-Full-bridge-INV system; (**d**) PV-Forward-Dbus compared with PV-Half-bridge-Dbus system.

Some conclusions can be drawn from Figure 10 and Table 9. Take the load resistance output as an example. When the weather parameters and the ratio are certain, the maximum value of the load resistance for the PV system using the forward converter as the MPPT circuit is about three times that for the PV system using the half-bridge converter. Meanwhile, the maximum value of the load resistance for the PV system using the full-bridge converter is about four times that for the PV system using the half-bridge converter. However, when $R_L < 4R_{sM}$, only the PV system using the half-bridge converter can successfully realize MPPT control. When the weather parameters and load resistance are certain, the maximum value of load resistance for the PV system using the full-bridge converter is about two times that for the PV system using the half-bridge converter. Meanwhile, only the PV system using the half-bridge converter can successfully realize MPPT control when $n < 0.28$. When an inverter is connected to the PV system, no matter what kind of converter is used as the MPPT control circuit, the range of circuit parameters is reduced to a certain extent. When the flyback converter is used, the load resistance, transformer ratio or bus voltage range is much larger than that of other isolated PV systems. Since both R_{sM} and V_{sM} are functions of S and T, the load, transformer ratio or bus voltage range changes with S and T. In addition, Figure 10 not only shows the range of variation in R_L, n and V_{Dbus} but also verifies the accuracy of the boundary values given in Table 9. The MPP linear model can be used only if the MPP is always present in the isolated PV system within this range.

In conclusion, both the different choices of isolated DC/DC converters and changing weather parameters may lead to changes in the MCCs.

3.3. Simulation Analysis of RMPPT

In order to verify the practicality of RMPPT and test its MPPT capability, the PV-Flyback system model was built by using Simulink. In this case, the MPP linear model in Section 2.1 is used. Meanwhile, n and R_L are equal to 2 and 1.7 Ω, respectively. In addition, the capacitors, inductors and transformers in the circuit are ideal components, the switching components are MOSFETs, and the PWM wave frequency is 15 kHz.

Simulation experiments on the practicality of RMPPT were conducted, and the results are shown in Table 10. D_{max} and D_{max1} denote D values at the MPP when the RMPPT and P&O methods are used, respectively. P_{omax} and P_{omax1} denote the maximum output power values of the PV cell when the RMPPT and P&O methods are used, respectively. P_{omax2} denotes the maximum output power of the PV system. The parameter settings are n = 1/10 and R_L = 500 Ω. The P&O method step size is set to 0.005.

Table 10. Experimental results for practicability of RMPPT.

(S,T)/(W/m^2, °C)	D_{max}	D_{max1}	P_{omax}	P_{omax1}	P_{omax2}
(750, 15)	0.4865	0.4821	152.19	152.13	149.63
(1000, 15)	0.5175	0.5204	214.7	214.89	212.5
(1250, 15)	0.54	0.5373	281.77	281.72	279.92
(750, 25)	0.4929	0.5007	151.29	151.22	148.79
(1000, 25)	0.524	0.5221	213.4	213.69	211.2
(1250, 25)	0.547	0.5455	280.87	280.83	277.93
(750, 35)	0.4994	0.5013	150.39	150.51	148.43
(1000, 35)	0.5308	0.5269	212.9	212.69	210.09
(1250, 35)	0.5539	0.5520	279.97	280.14	277.64

In Table 10, it can be seen that the values of D_{max} and P_{omax} calculated by RMPPT are basically equal to D_{max1} and P_{max1}, respectively. This proves the practicality of RMPPT. In addition, it can be seen from P_{omax1} and P_{omax2} that there is a difference between them due to the loss of the circuit components, the average value of which is the circuit loss, which is calculated to be about 2.41W.

Two sets of simulation experiments were performed for RMPPT using Simulink. And the MPPT methods were judged on the basis of stability and speed.

(1) Simulation experiment of irradiance change

In order to simulate a sudden weather change situation, it is assumed that at 0~0.3 s, S = 800 W/m^2 and T = 25 °C; at 0.3~0.7 s, S = 1200 W/m^2 and T = 25 °C; and at 0.7~1 s, S = 400 W/m^2 and T = 25 °C. Figure 11 shows the simulation results.

In Figure 11b, it can be seen that the tracking time and numerical stability of the MPP are much better than in the traditional P&O method when RMPPT is used in the isolated PV system with sudden changes in weather conditions (S). In Figure 11c, it can be seen that the P&O method itself has a step-length limitation, which causes D to oscillate around D_{max}, which is the reason why the output power of the P&O method oscillates at the MPP, while the RMPPT stabilizes at the MPP. It can also be seen in Figure 11 that, after the sudden change in S, D is actively adjusted to the new D_{max}, and the P_{omax} of the PV cell is also stabilized to the new P_{omax} after a rapid adjustment, which also proves the correctness of the conclusion in Section 2.1.

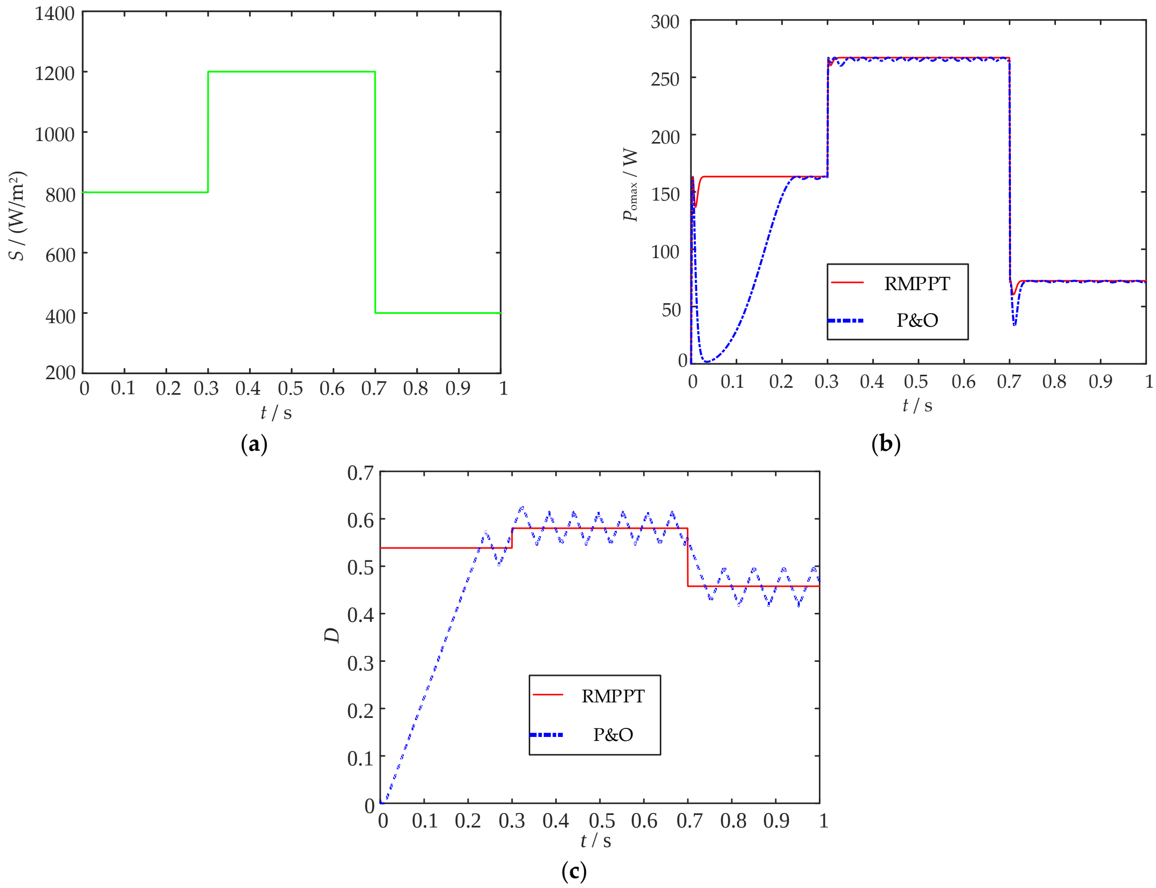

Figure 11. Simulation experiment of irradiance change. (**a**) S curve variation with t; (**b**) comparison of P_{omax}-t curves of RMPPT and P&O methods; (**c**) comparison of D-t curves of RMPPT and P&O methods.

(2) Simulation experiment of R_L change

Figure 12 shows the simulation results. In Figure 12b, it can be seen that the tracking time and numerical stability of the MPP are much better than those of the P&O method when RMPPT is used with sudden changes in R_L. It can also be seen in Figure 12 that D_{max} is actively adjusted to the new D_{max} after a sudden change in R_L, but P_{omax} remains at the same value after a short transient adjustment.

Therefore, it can be concluded that RMPPT outperforms the conventional P&O method in terms of MPPT rapidity and stability, regardless of changing weather conditions or circuit parameters.

Although only the MPPT method for the PV-Flyback system based on Equation (62) is proposed and verified in this section, the remaining MPPT methods for different isolated PV systems can be proposed analogously, which makes it easy for researchers and users of PV systems to select the corresponding MPPT methods.

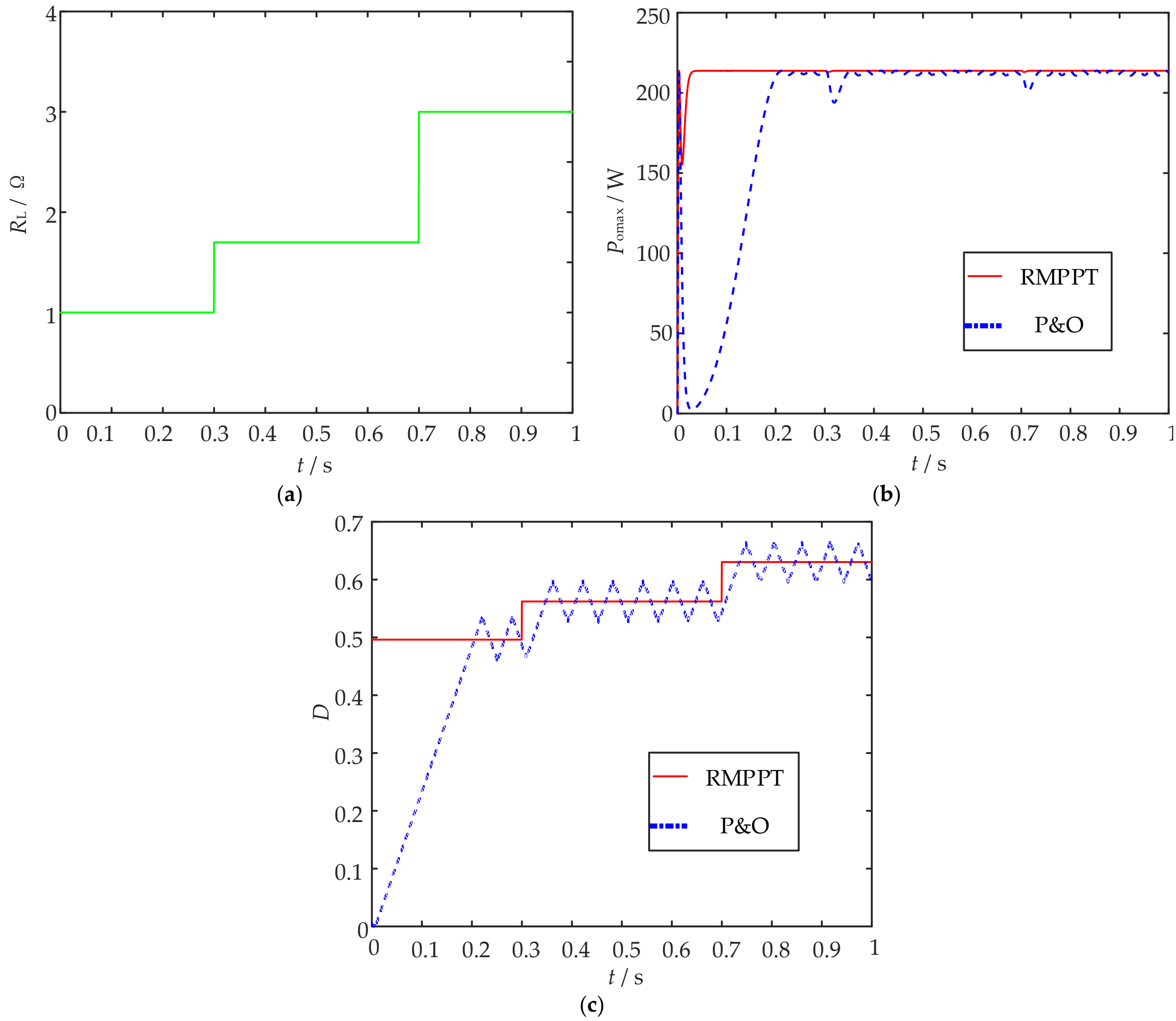

Figure 12. Simulation experiment of R_L change. (**a**) R_L curve variation with t; (**b**) comparison of P_{omax}-t curves of RMPPT and P&O methods; (**c**) comparison of D-t curves of RMPPT and P&O methods.

3.4. Simulation Analysis of BMPPT

In order to verify the practicality of BMPPT and test its MPPT capability, the PV-Flyback-Dbus system model shown in Figure 8 was built by using Simulink. The parameter settings are n = 2 and V_{Dbus} = 25 V, the capacitors, inductors and transformers in the circuit are ideal components, the switching components are MOSFETs, and the PWM wave frequency is 15 kHz. The simulation experiment results under varying temperature and DC bus voltage conditions are shown in Figure 13.

In Figure 13b,e, it can be seen that the tracking time and numerical stability of the MPP are much better than in the P&O method when BMPPT is used in isolated PV systems with sudden changes in T or V_{Dbus}. It can also be seen in Figure 13b,c that, after a sudden change in T, D_{max} is actively adjusted to the new D_{max}, and P_{omax} is also stabilized to the new P_{omax} after a rapid stepwise adjustment.

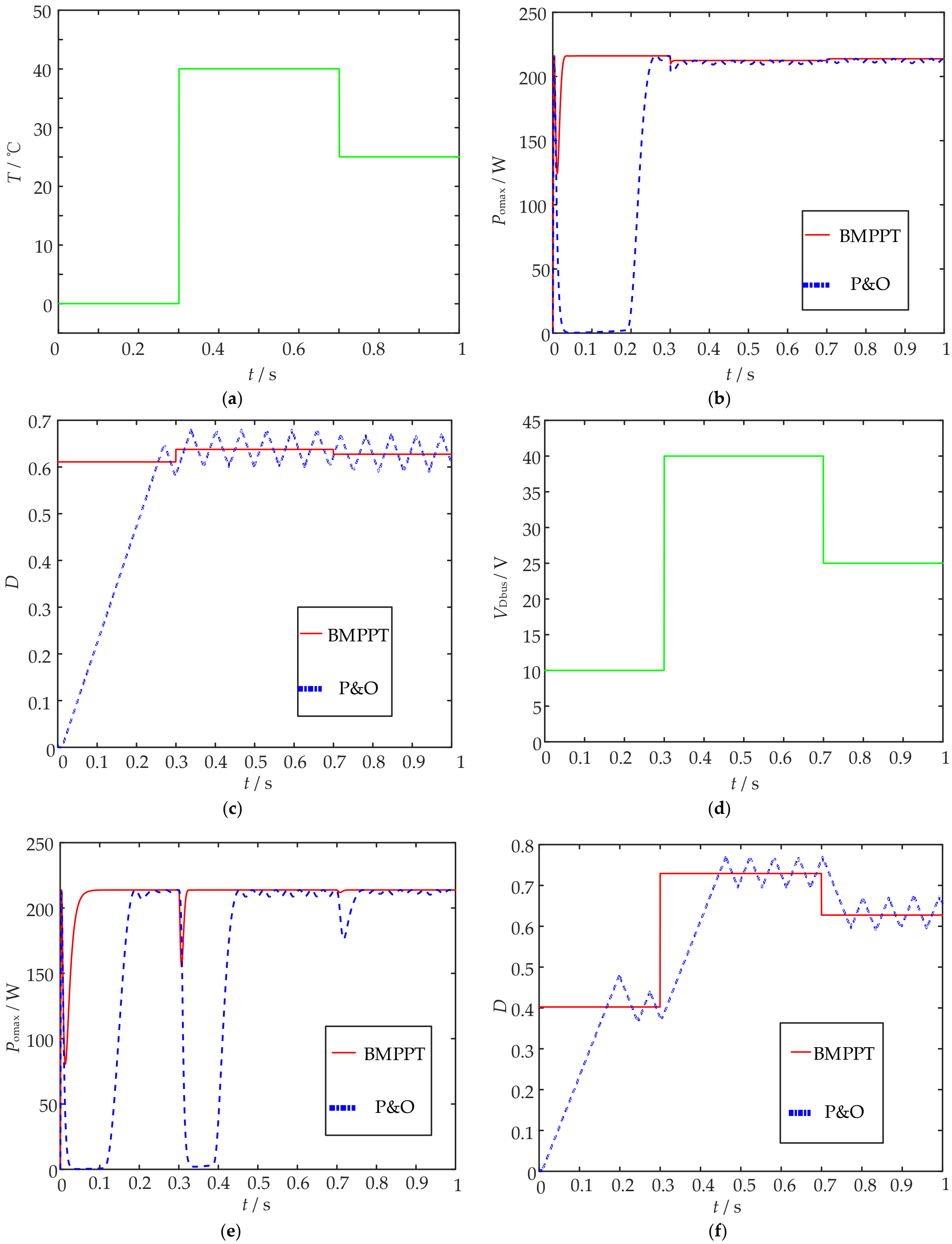

Figure 13. Simulation experiment of T and V_{Dbus} changes. (**a**) T curve variation with t; (**b**) comparison of P_{omax}-t curves of T change; (**c**) comparison of D-t curves of T change; (**d**) V_{Dbus} curve variation with t; (**e**) comparison of P_{omax}-t curves of V_{Dbus} change; (**f**) comparison of D-t curves of V_{Dbus} change.

Therefore, it can be concluded that BMPPT is far superior to the traditional P&O method in terms of rapidity and stability under changing weather conditions or circuit parameters.

Although only the MPPT method for the PV-Flyback-Dbus system based on the theory of Equation (63) is proposed and validated in this section, the remaining MPPT methods for different isolated PV systems can also be proposed analogously.

In this section, two MPPT methods (RMPPT and BMPPT) are verified when a load resistance and DC bus are selected as the output of the PV system, respectively. The conventional P&O method is compared with two MPPT methods implemented in Matlab/Simulink under varying weather conditions (irradiance and temperature) and circuit parameters (DC bus voltage and load resistance). The experimental results verify the high speed and accuracy of the two proposed MPPT methods and show the advantages of a simple program, small computational volume and low cost of hardware and software. They also verify the correctness and practicability of the MPP linear model established in Section 2.1.

4. Discussion

Tables 1–5 show the constraint conditions that enable the successful realization of MPPT control for isolated PV systems on the basis of the PV cell engineering model and MPP linear model. However, in practical applications, these constraint conditions usually play an important role in the hardware design, theoretical study and product installation of the PV system. On the one hand, since the boundaries of these constraints always change with the weather parameters, it is difficult to adjust the operating system in real time based on whether the load (or bus voltage) varies within the MCC range. For hardware designers, the MCCs can be utilized to select system configurations and circuit components. For the theoretical researcher, the MCCs can be used as a basis for ensuring the usability of the proposed control method. For the system installer, the MCCs can be used to estimate the MPPT effect based on solar irradiance and temperature recordings in the installation area. On the other hand, in practical applications, the maximum selected value of the load (or bus voltage) can be reflected by the MCCs. In other words, for a PV system, if the selected value of the load (or bus voltage) is not within the corresponding interval, the MPP cannot be successfully tracked, regardless of the used MPPT method, in which case, of course, the MPP linear model cannot be used. In addition, the MCCs can provide a theoretical basis when the MPP linear model is used to study the overall linearized model of the PV system.

However, in practice, the MPPT control of PV systems is usually affected by some other factors, such as the installed PV power, non-ideal DC/DC converter, non-ideal inverter and transmission efficiency. Therefore, the conclusions of this paper will be influenced by these factors to some extent. However, these factors are negligible. The reasons are as follows. On the one hand, the use of ideal isolated DC/DC converters and inverters can greatly simplify the theoretical study, just like in other studies. On the other hand, the aim of this work is to reveal the governing relationships between PV cell parameters and the load resistance or bus voltage when the MPP of the PV system is always present. Obviously, obtaining these relationships is very beneficial for the study of MPPT control methods using both PV cell models. Finally, the two constraint conditions in this paper represent the key results on the basis of which other factors can be easily considered and involved in practical applications.

5. Conclusions

For isolated PV systems, this paper solves the problem of when to apply the MPP linear model of the PV cell and proposes two faster and more accurate MPPT methods on the basis of MCCs, which are important for studying the overall linearization of isolated PV systems. In practical applications, the MCCs are a good guide for the circuit design, theoretical derivation and product selection of isolated PV systems. Theoretical researchers, hardware circuit designers and PV equipment installers can select the suitable isolated PV system according to different load and DC bus range requirements and make a preliminary estimation of MPPT effects. The main work in this paper is summarized as follows:

(1) The overall mathematical models of twenty isolated PV systems are established. And the relationships between the output power of isolated PV systems, the parameters of the PV cell and circuit parameters are found.
(2) The MCCs are found for isolated PV systems with different topologies and outputs on the basis of the PV cell engineering model and MPP linear model, respectively. They are a good guide for the circuit design, theoretical derivation and product selection of PV systems.
(3) Based on the MPP linear model and MCC, two MPPT methods (RMPPT and BMPPT) applicable to different output conditions are proposed. The experimental results verify the speed and accuracy of the two proposed MPPT methods. The MPPT time is improved from 0.23 s to 0.03 s. These two methods have the advantages of a simple program, small computational volume and low hardware and software costs.

Although this thesis finds some direct mathematical relationships between weather parameters (irradiance and temperature), circuit parameters (load resistance, transformer ratio and bus voltage) and control signals (PWM wave duty cycle) for isolated PV systems and proposes two MPPT methods applicable to different topologies and load types, there is still a lot of follow-up work to be carried out.

(1) The theoretical derivation in this paper makes some idealized assumptions. However, there may be more complicated situations in the practical circuit, and determining how to establish the MCCs and MPPT methods for more complicated situations is an important research direction.
(2) The two MPPT methods proposed put forward higher requirements on the speed, accuracy and economy of the irradiance and temperature sensors. If irradiance and temperature sensors with lower costs, higher accuracy and faster speed can be developed, the MPPT control method proposed in this paper can be more widely used.
(3) The MCCs proposed in this paper are based on the premise that the irradiance of all PV cells is uniform, but due to the environmental changes that may occur in the case of the partial shading of PV cells, it is also an important direction to consider the MCCs and the MPPT method in the case of non-uniform irradiance.

Author Contributions: Conceptualization, J.F. and S.L. (Shaowu Li); methodology, J.F.; software, J.F.; validation, J.F., S.L. (Shaowu Li), S.L. (Sanjun Liu) and X.Z.; formal analysis, J.F.; investigation, J.F., S.L. (Shaowu Li), S.L. (Sanjun Liu), X.D. and X.Z.; resources, S.L. (Shaowu Li) and S.L. (Sanjun Liu); data curation, J.F.; writing—original draft preparation, J.F. and S.L. (Shaowu Li); writing—review and editing, J.F., S.L. (Shaowu Li) and S.L. (Sanjun Liu); visualization, J.F. and S.L. (Shaowu Li); supervision, S.L. (Shaowu Li), S.L. (Sanjun Liu), X.D. and X.Z.; project administration, S.L. (Shaowu Li) and S.L. (Sanjun Liu); funding acquisition, S.L. (Shaowu Li), S.L. (Sanjun Liu) and X.D. All authors have read and agreed to the published version of the manuscript.

Funding: This research was funded by the National Natural Science Foundation of China (Nos. 61961016 and 61963014).

Data Availability Statement: All relevant data are within the paper.

Acknowledgments: The authors would like to sincerely thank the editor and anonymous reviewers for their valuable comments and suggestions to improve the quality of the article.

Conflicts of Interest: Author J.F. was employed by the company Jiangmen Pengjiang Power Supply Bureau of Guangdong Power Grid Co., Ltd. Author X.D. was employed by the company Hubei Chuangsinuo Electrical Technology Corp. Author X.Z. was employed by the company Guilin Power Supply Bureau of Guangxi Power Grid Co., Ltd. The remaining authors declare that the research was conducted in the absence of any commercial or financial relationships that could be construed as a potential conflict of interest.

Abbreviations

MPP	Maximum power point	STC	Standard test conditions
PV	Photovoltaic	PWM	Pulse-width modulation
MCC	MPPT constraint conditions	DC	Direct current
MPPT	Maximum power point tracking	AC	Alternating current
VWP	Variable-weather parameter		

Nomenclature

I	Output current of PV cell (A)	n	Transformer ratio of isolated DC/DC converter
V	Output voltage of PV cell (V)	M	SPWM wave modulation ratio
S	Solar irradiance (W/m^2)	V_r	Output voltage of inverter (V)
T	Cell temperature (°C)	I_r	Output current of inverter (A)
I_o	Output current of isolated DC/DC converter (A)	R_{sM}	Internal resistance of linear cell model (Ω)
V_o	Output voltage of isolated DC/DC converter (V)	V_{sM}	Open-circuit voltage of MPP linear model (V)
D	Duty cycle of the PWM signal of converter	D_{max}	D at the MPP
I_{sc}	Short-circuit current of PV cell under STC (A)	P_{omax}	Output power at MPP (W)
V_{oc}	Open-circuit voltage of PV cell under STC (V)	R_{iMPP}	Value of R_i at MPP (Ω)
I_m	MPP current of PV cell under STC (A)	V_{MPP}	Value of V at MPP (Ω)
V_m	MPP voltage of PV cell under STC (V)	I_{MPP}	Value of I at MPP (Ω)
R_i	Input resistance of isolated DC/DC converter (Ω)	V_{Dbus}	Voltage of DC bus (V)
R_L	Load or equivalent load resistance of PV system (Ω)	V_{Abus}	Voltage of AC bus (V)
D_{L1}	Minimum D for forward and flyback converters	D_{L2}	Minimum D for half-bridge, full-bridge, push–pull converter
D_{U1}	Maximum D for forward and flyback converters	D_{U2}	Maximum D for half-bridge, full-bridge, push–pull converter
P_o	Output power of PV system (W)		

References

1. Zhao, D.; Qian, M.; Ma, J.; Yamashita, K. Photovoltaic generator model for power system dynamic studies. *Sol. Energy* **2020**, *210*, 101–114. [CrossRef]
2. Koohi-Kamali, S.; Rahim, N.A.; Mokhlis, H.; Tyagi, V.V. Photovoltaic electricity generator dynamic modeling methods for smart grid applications: A review. *Renew. Sustain. Energy Rev.* **2016**, *57*, 131–172. [CrossRef]
3. Moreira, H.S.; Silva, J.L.D.S.; Reis, M.V.G.D.; Mesquita, D.B.; Paula, B.H.K.; Villalva, M.G. Experimental comparative study of photovoltaic models for uniform and partially shading conditions. *Renew. Energy* **2021**, *164*, 58–73. [CrossRef]
4. Li, Q.; Zhao, S.; Wang, M.; Zou, Z.; Wang, B.; Chen, Q. An improved perturbation and observation maximum power point tracking algorithm based on a PV module four-parameter model for higher efficiency. *Appl. Energy* **2017**, *195*, 523–537. [CrossRef]
5. Yin, O.W.; Babu, B.C. Simple and easy approach for mathematical analysis of photovoltaic (PV) module under normal and partial shading conditions. *Optik* **2018**, *169*, 48–61. [CrossRef]
6. Zsiborács, H.; Baranyai, N.H.; Vincze, A.; Pintér, G. An economic analysis of the shading effects of transmission lines on photovoltaic power plant investment decisions: A case study. *Sensors* **2021**, *21*, 4973. [CrossRef]
7. Hsieh, Y.; Yu, L.; Chang, T.; Liu, W.; Wu, T.; Moo, C. Parameter identification of one-diode dynamic equivalent circuit model for photovoltaic panel. *IEEE J. Photovolt.* **2020**, *10*, 219–225. [CrossRef]
8. Si, X.; Chen, Q.; Gao, Z. A piecewise linearization based equivalent model of photovoltaic array. *Power Syst. Technol.* **2014**, *38*, 947–951.
9. Wang, Y.J.; Hsu, P.C. Modelling of solar cells and modules using piecewise linear parallel branches. *IET Renew. Power Gener.* **2011**, *5*, 215–222. [CrossRef]
10. Bharadwaj, P.; John, V. Linearised model for PV panel power output variation with changes in ambient conditions. *Sādhanā* **2017**, *42*, 2183–2187. [CrossRef]
11. Golshani, A.; Bathaee, S.M.T.; Moghaddas-Tafreshi, S.M. Small signal stability analysis of photovoltaic array based on averaged switch modeling technique. *J. Renew. Sustain. Energy* **2012**, *4*, 043117. [CrossRef]
12. Li, S. Linear equivalent models at the maximum power point based on variable weather parameters for photovoltaic cell. *Appl. Energy* **2016**, *182*, 94–104. [CrossRef]
13. Amir, A.; Amir, A.; Che, H.S.; Khateb, A.E.; Rahim, N.A. Comparative analysis of high voltage gain DC-DC converter topologies for photovoltaic systems. *Renew. Energy* **2019**, *136*, 1147–1163. [CrossRef]
14. Başoğlu, M.E.; Çakır, B. Comparisons of MPPT performances of isolated and non-isolated DC-DC converters by using a new approach. *Renew. Sustain. Energy Rev.* **2016**, *60*, 1100–1113. [CrossRef]
15. Brito, M.A.G.; Galotto, L.; Sampaio, L.P.; Melo, G.A.; Canesin, C.A. Evaluation of the main MPPT techniques for photovoltaic applications. *IEEE Trans. Ind. Electron.* **2013**, *60*, 1156–1167. [CrossRef]

16. Seyedmahmoudian, M.; Horan, B.; Soon, T.K.; Rahmani, R.; Oo, A.M.T.; Mekhilef, S.; Stojcevski, A. State of the art artificial intelligence-based MPPT techniques for mitigating partial shading effects on PV systems—A review. *Renew. Sustain. Energy Rev.* **2016**, *64*, 435–455. [CrossRef]
17. Hassan, T.U.; Abbassi, R.; Jerbi, H. A novel algorithm for MPPT of an isolated PV system using push pull converter with fuzzy logic controller. *Energies* **2020**, *13*, 4007. [CrossRef]
18. Islam, H.; Mekhilef, S.; Shah, N.B.M.; Soon, T.K.; Seyedmahmousian, M.; Horan, B.; Stojcevski, A. Performance evaluation of maximum power point tracking approaches and photovoltaic systems. *Energies* **2018**, *11*, 365. [CrossRef]
19. Bollipo, R.B.; Mikkili, S.; Bonthagorla, P.K. Hybrid, optimization, intelligent and classical PV MPPT techniques: Review. *CSEE J. Power Energy Syst.* **2021**, *7*, 25.
20. Mohapatra, A.; Nayak, B.; Das, P.; Mohanty, K.B. A review on MPPT techniques of PV system under partial shading condition. *Renew. Sustain. Energy Rev.* **2017**, *80*, 854–867. [CrossRef]
21. Li, S.; Ping, A.; Liu, Y.; Ma, X.; Li, C. A variable-weather-parameter MPPT method based on a defined characteristic resistance of photovoltaic cell. *Sol. Energy* **2020**, *199*, 673–684. [CrossRef]
22. Li, S. Circuit parameter range of photovoltaic system to correctly use the mpp linear model of photovoltaic cell. *Energies* **2021**, *14*, 3997. [CrossRef]
23. Chen, J.; Kang, Y. *Power Electronics: Power Electronic Conversion and Control Technology*, 3rd ed.; Higher Education Press: Beijing, China, 2011; pp. 81–93.
24. Qiu, G.; Luo, X. *Circuits*, 5th ed.; Higher Education Press: Beijing, China, 2013.

Disclaimer/Publisher's Note: The statements, opinions and data contained in all publications are solely those of the individual author(s) and contributor(s) and not of MDPI and/or the editor(s). MDPI and/or the editor(s) disclaim responsibility for any injury to people or property resulting from any ideas, methods, instructions or products referred to in the content.